Morphology, volcanism, and mass wasting in Crater Lake, Oregon

Charles R. Bacon*
Volcano Hazards, U.S. Geological Survey, 345 Middlefield Road, MS 910, Menlo Park, California 94025-3591, USA

James V. Gardner
Western Coastal and Marine Geology, U.S. Geological Survey, 345 Middlefield Road, M.S. 999, Menlo Park, California 94025-3591, USA

Larry A. Mayer
Center for Coastal and Ocean Mapping, University of New Hampshire, 24 Colovos Road, Durham, New Hampshire 03824, USA

Mark W. Buktenica
National Park Service, Crater Lake National Park, P.O. Box 7, Crater Lake, Oregon 97604, USA

Peter Dartnell
Western Coastal and Marine Geology, U.S. Geological Survey, 345 Middlefield Road, M.S. 999, Menlo Park, California 94025-3591, USA

David W. Ramsey
Joel E. Robinson
Volcano Hazards, U.S. Geological Survey, 345 Middlefield Road, M.S. 910, Menlo Park, California 94025-3591, USA

ABSTRACT

Crater Lake was surveyed nearly to its shoreline by high-resolution multibeam echo sounding in order to define its geologic history and provide an accurate base map for research and monitoring surveys. The bathymetry and acoustic backscatter reveal the character of landforms and lead to a chronology for the concurrent filling of the lake and volcanism within the ca. 7700 calibrated yr B.P. caldera. The andesitic Wizard Island and central-platform volcanoes are composed of sequences of lava deltas that record former lake levels and demonstrate simultaneous activity at the two vents. Wizard Island eruptions ceased when the lake was ~80 m lower than at present. Lava streams from prominent channels on the surface of the central platform descended to feed extensive subaqueous flow fields on the caldera floor. The Wizard Island and central-platform volcanoes, andesitic Merriam Cone, and a newly discovered probable lava flow on the eastern floor of the lake apparently date from within a few hundred years of caldera collapse, whereas a small rhyodacite dome was emplaced on the flank of Wizard Island at ca. 4800 cal. yr B.P. Bedrock outcrops on the submerged caldera walls are shown in detail and, in some cases, can be correlated with exposed geologic units of Mount Mazama. Fragmental debris making up the walls elsewhere consists of narrow talus cones forming a dendritic pattern that leads to fewer, wider ridges downslope. Hummocky topography and scattered blocks up to ~280 m long below many of the embayments in the caldera wall mark debris-avalanche deposits that probably formed in single events and commonly are affected by secondary failures. The flat-floored, deep basins contain relatively fine-grained sediment transported from the debris aprons by sheet-flow turbidity currents. Crater Lake apparently filled rapidly (ca. 400–750 yr) until reaching a permeable layer above glaciated lava identified by the new survey in the northeast caldera wall at ~1845 m elevation. Thereafter, a gradual, climatically modulated rise in lake level to the present 1883 m produced a series of beaches culminating in a modern wave-cut platform, commonly ~40 m wide, where suitable material is present. The new survey reveals landforms that result from intermediate-composition volcanism in rising water, delineates mass wasting and sediment transport into a restricted basin, and yields a more accurate postcaldera history leading to improved assessment of volcanic hazards.

Keywords: bathymetry, calderas, Crater Lake, limnology, mass wasting, volcanology.

INTRODUCTION

Crater Lake partially fills the caldera that collapsed at ca. 7700 cal. yr B.P. during the climactic eruption of Mount Mazama, an andesite-dacite stratovolcano in the Cascades. Crater Lake is the deepest in the United States and is known for its exceptional clarity and cobalt blue color. The cinder cone and lava flows of Wizard Island attest to volcanic activity since the caldera formed and hint at a volcanic landscape hidden beneath the lake. Armed with piano wire and a weight, an 1886 U.S. Geological Survey party made 186 soundings and determined that the lake was nearly 2000 feet deep. Additional wireline soundings were made in 1938–1940 by the National Park Service. The U.S. Coast and Geodetic Survey obtained >4000 acoustic soundings in 1959. Con-

*E-mail: cbacon@usgs.gov.

GSA Bulletin; June 2002; v. 114; no. 6; p. 675–692; 14 figures; 2 tables.

tours of the echo-sounding data by Williams (1961) and Byrne (1962, 1965) revealed the principal morphologic features of the floor of Crater Lake. However, in the vicinity of the caldera walls and volcanic hills, the wide-angle echo-sounding method led to underestimation of depths and slopes directly beneath the vessel. Exploration of the lake floor with the manned submersible *Deep Rover* in 1988 and 1989 (Collier et al., 1991) confirmed the inaccuracy of the existing bathymetric map and pointed out the need for remapping the bathymetry of Crater Lake with modern techniques, both to provide a key element in the interpretation of postcaldera geologic history and to establish a base for further study of the lake itself.

Crater Lake was resurveyed nearly to its shoreline during five days in July and August 2000 by a team from the U.S. Geological Survey (USGS), the University of New Hampshire, C and C Technologies, Inc., and the National Park Service (Gardner et al., 2001; additional images of Crater Lake can be found at http://walrus.wr.usgs.gov/pacmaps). As in the 1998 survey of Lake Tahoe (Gardner et al., 2000a), a system was used that included a high-resolution multibeam echo sounder (MBES), a vehicle-motion sensor with inertial navigator, and a dual-differential Global Positioning System (DGPS) navigation system. These were mounted on the 8 m *Surf Surveyor* that was transported into and out of Crater Lake caldera by a U.S. Army Reserve CH-47D Chinook helicopter from Fort Lewis, Washington. The 2000 survey collected >16 million soundings accurate to 0.2% of water depth and geographically referenced by using positioning methods for which the accuracy is better than ±1 m. Here, we present maps of the detailed morphology and acoustic backscatter of Crater Lake, discuss volcanic and sedimentary processes that shaped the lake floor, and describe the geologic history of Crater Lake caldera following the climactic eruption of Mount Mazama.

METHODS

The 2000 survey used a boat specifically designed for a hull-mounted Kongsberg Simrad EM1002 MBES. The EM1002 system operates at frequencies of 98 kHz (inner ± 50° swath centered at nadir) and 93 kHz (the outer ± 25°). The system transmits a narrow along-track, wide across-track pulse and then receives backscattered energy with 111 receive apertures (2° × 2°) that are distributed across track. A bathymetric sounding is derived for each beam, as is a coregistered acoustic-backscatter-energy level calibrated to the energy of the transmitted pulse at 1 m out from the transducer. Vehicle motion was measured by using a TSS POS/MV model 320 sensor that provides roll, pitch, and heave with accuracies of 0.05° as well as true heading to 0.5°. Positions were provided by a dual-differential GPS–aided inertial navigation system. The navigation system's accuracy was measured against established USGS bench marks along the shore of Crater Lake and was found to provide horizontal-position accuracy of better than ±1 m. Vertical sound-velocity profiles for the lake were determined by using a SeaBird CTD (conductivity, temperature, and depth instrument) and (periodically) expendable bathythermographs. Sound velocity at the transducer was continuously measured by two fixed sound-velocity sensors. Sound-velocity profiles were used to individually ray-trace each sounding from each beam to correctly locate the sounding on the lake floor. All of the attitude and sound-velocity data were networked to the Kongsberg Simrad processor for accurate beam forming and preprocessing. The survey was run at ~8 kts (knots) during daylight hours, and all of the data were processed in the field. Specific details of the systems and processing can be found in Gardner et al. (2000b). When properly compensated, the depth accuracy of the EM1002 system is 0.2% of water depth or 10 cm, whichever is greater. All measured depths were referenced to the lake level (1882.6 m) as measured by a USGS lake gauge (station number 11492200) on the north shore of Crater Lake (numbers in Gardner et al. [2000b] are incorrect). Measured lake depths were converted to elevations above mean sea level to provide a continuous digital elevation model for Crater Lake caldera. The individual point data were gridded at 2 m spatial resolution for the entire lake floor by using the WGS84 ellipsoid for the horizontal datum.

TABLE 1. CALCULATED AREAS AND VOLUMES

Feature	Area (km²)	Volume (km³)
Crater Lake	53.4	18.7
Hypothetical lake to 2050 m elevation	60.4	28.2
Central-platform edifice	3.19	0.758
Central-platform lava flow fields	4.89	0.300
Wizard Island, subaerial	1.22	0.064
Wizard Island, above 1805 m elevation	4.60	0.262
Wizard Island, above 1700 m elevation	6.08	0.817
Wizard Island, above 1550 m elevation	7.95	1.880
Wizard Island, entire edifice	8.97	2.62
Merriam Cone	2.38	0.342
East basin lava(?)	0.87	0.032
Total postcaldera andesite	20.3	4.05
Rhyodacite dome	0.61	0.074
Chaski Bay debris-avalanche deposit	4.56	0.224
Chaski Bay slump deposit	0.035	0.0004
Debris-avalanche deposit west of Eagle Point	0.58	0.013
Danger Bay, west debris-avalanche deposit	1.26	0.038
Danger Bay, east debris-avalanche deposit	1.15	0.034
Cloudcap Bay debris-avalanche deposit	0.58	0.0024
Grotto Cove, deep slide	0.14	0.0015
Steel Bay, deep slide	0.26	0.0027
Llao Bay debris-avalanche deposit	0.72	0.014

In addition to bathymetry, the EM1002 system also records a time series of the strength of acoustic-backscatter energy from each beam footprint. When pieced together, these backscatter time series produce imagery (measured in decibels [dB]) that is similar in appearance to a sidescan-sonar record. The system and processing software corrects the energy received at each beam for source-level gain changes, grazing angle, propagation losses, predicted and measured beam pattern, and the insonified area. Each −3 dB change in backscatter represents a 50% decrease in received energy. Backscatter is a function of a combination of acoustic impedance contrast, surface roughness, and volume reverberation within the area of the individual beam footprint (a few square meters) and from an unknown and variable thickness (probably on the order of <25 cm) of sediment. A map of backscatter can be loosely interpreted as some indication of the physical characteristics of the lake floor (Gardner et al., 1991; Hughes Clarke, 1993).

The volumes of geologic features within Crater Lake (e.g., Wizard Island volcano, landslides) were calculated by using the GIS software package ArcInfo (Table 1). The hidden caldera floor and walls that form a surface beneath these features were modeled as follows. The multibeam data were desampled from 2 m resolution to 20 m resolution and 50 m isobaths were generated. The resulting contour file was converted to a shape file and imported into Adobe Illustrator with the MAPublisher plug-in. Contours on the caldera floor were rearranged to approximate the acoustic basement surface of Nelson et al. (1988). This file was imported back into ArcInfo, and a new basement surface was generated. Volumes of geologic features were calculated as the difference between the modern and basement surfaces by using the ArcInfo cutfill command.

DEPTH AND VOLUME OF CRATER LAKE

We report bathymetric data as elevations rather than depths because the level of Crater Lake has varied historically (Redmond, 1990). The lake surface had an elevation of 1882.6 m (6176.5 feet) during the 2000 survey. We found the maximum depth of 593.5 ± 1.2 m (1947.2 ± 3.9 feet) in the east basin, or a minimum elevation of 1289.1 m for the lake floor. Formerly, the maximum depth was reported as 589 m (1932 feet; Byrne, 1962), referenced to an elevation of 1882.4 m (6176 feet). The range in surface elevation of Crater Lake for the 1892 through 2000 period of record was 1878.5 m (6163.2 feet; 1942) to 1883.5 m (6179.3 feet; 1975), and the mean value is 1881.5 m (6172.9 feet), which gives a mean maximum depth of 592.4 m (1943.6 feet). We prefer to state the maximum depth as 594.0 m (1949 feet) relative to the elevation of 6178 feet that appears on U.S. Geological Survey 1:24 000-scale topographic maps. In North America, only Great Slave Lake is deeper than Crater Lake.

Previous estimates of the volume of Crater Lake were 16 km^3 (Byrne, 1965; value appears to have a calculating error) and 17.3 km^3 (Phillips, 1968). Our calculated lake volume of 18.7 km^3 (Table 1) is larger because of improved accuracy of depth soundings, particularly near the caldera walls, and is more precise because of the vastly increased number of soundings. The area of the lake is 53.4 km^2 calculated from a USGS digital shoreline file.

GEOLOGY OF MOUNT MAZAMA

The geology of Mount Mazama is of interest here not only to provide a context for interpretation of its postcaldera history as revealed by lake-floor morphology but also to extend geologic mapping to submerged caldera-wall exposures. The general geology of Mount Mazama was described in monographs by Diller and Patton (1902) and Williams (1942). The caldera was shown to be a collapse feature, linked by Williams to explosive eruption of a large volume of gas-rich magma represented by pyroclastic-fall and -flow deposits. Renewed study of the geology of Mount Mazama since about 1980 has greatly expanded knowledge of its eruptive history, petrology, geochemistry, and physical volcanology (Bacon, 1983; Bacon and Lanphere, 1990; publications listed at http://craterlake.wr.usgs.gov/bibliography.html).

Mount Mazama consisted of a cluster of overlapping andesitic to dacitic composite cones, shield volcanoes, and flank lava flows constructed between ca. 420 ka and ca. 35 ka. Collapse of the summit of this edifice in the caldera-forming, or climactic, eruption at ca. 7700 cal. yr B.P. left the flanks of Mount Mazama and remnants of its slopes outside of the caldera rim. Its eruptive history has been determined by detailed geologic mapping of the flank and caldera-wall exposures and by a comprehensive program of K-Ar and Ar-Ar geochronology (C.R. Bacon and M.A. Lanphere, unpublished data, 2000). The eruptive center migrated from east to west during the lifetime of Mount Mazama. Its final products were dacitic summit domes, represented now by the ca. 35 ka dome-collapse deposits on the southwest flank of Mazama. Subsequently, several rhyodacite lava flows and domes, fed from the growing upper-crustal climactic magma chamber, were emplaced north and east of the ~4000 m summit. The youngest of these rhyodacitic lava flows was still hot when the caldera collapsed. The zoned climactic eruption vented ~50 km^3 of vapor-saturated, dominantly rhyodacitic and subordinate andesitic magmas and cumulate mush, preserved in extensive pumice-fall and thick pyroclastic-flow deposits. Postcaldera volcanism was confined to the caldera and was dominated by andesite. At various times throughout Mazama's history, hydrothermal systems within and beneath the edifice variably altered its constituents to propylitic assemblages.

Beneath Mount Mazama's southeast, east, and northeast flanks are extensive ca. 470 to ca. 420 ka rhyodacitic lava flows and domes. On the southwest flank, and likely west and north, Mazama is underlain by regional basaltic and basaltic andesitic lavas of the High Cascades. Similar lavas were erupted from vents peripheral to Mazama throughout the Quaternary, including into the Holocene. Widespread mafic volcanism was facilitated by the mildly extensional tectonic environment of the southern Cascades. The geology at greater depth near Mount Mazama is known from two geothermal exploration wells east and south of Crater Lake National Park (Bacon and Nathenson, 1996). Andesite and dacite lava and breccia, basaltic andesitic lava, and silicic pyroclastic rocks were cored at the eastern well, and basaltic andesitic lava and a probable sill were cored at the southern site. Some of the deepest caldera-wall exposures may correlate with intermediate-composition rocks recovered from the eastern well.

The geology of the floor of Crater Lake was inferred by Williams (1961) from the 1959 echo-sounding survey and dredge samples provided by C.H. Nelson. Nelson and coworkers have described the sediments of the lake floor and sedimentary processes in the lake on the basis of core samples (Nelson, 1967) and seismic reflection profiling (Nelson et al., 1986, 1988, 1994). Heat-flow measurements (Williams and Von Herzen, 1983) delineated areas of high convective heat flux, which were explored in 1987–1989 by Oregon State University and National Park Service scientists using a remotely operated vehicle (ROV) and the manned submersible *Deep Rover* (Collier et al., 1991). The latter also was used to explore and sample postcaldera volcanic features and outcrops on the submerged caldera walls (Nelson et al., 1994). Results of these studies aid and corroborate interpretation of the new bathymetric and backscatter data.

MORPHOLOGY AND BACKSCATTER OF CRATER LAKE FLOOR

The major volcanic and sedimentary features of the floor of Crater Lake were known prior to the present survey. However, their morphology was not known with sufficient detail to permit accurate interpretations of their origin or the relative ages of different geologic units. The high spatial and depth resolution of the new data (Fig. 1), coupled with acoustic backscatter intensity (Fig. 2), more clearly defines the character of landforms and leads to a chronology for the concurrent filling of Crater Lake and volcanism within the caldera. Although we have attempted to portray the features described in this paper in the figures, the reader should be aware that our measurements and interpretations were made with maps and perspective scenes at higher magnification than can be reproduced here.

Volcanic Features

The volcanoes on the floor of Crater Lake date from after collapse of the caldera. Their composition and general character are known from the sampling and exploration previously noted (e.g., Nelson et al., 1994). The new survey clarifies uncertainty about their mode of eruption, relative ages, and the extent of lava fields.

Wizard Island Volcano

Viewed from the caldera rim, the cinder cone and exposed lava flows of the Wizard Island volcano belie the bulk of this postcaldera edifice (Fig. 1). Its summit is a full 750 m above its deepest point, it has a

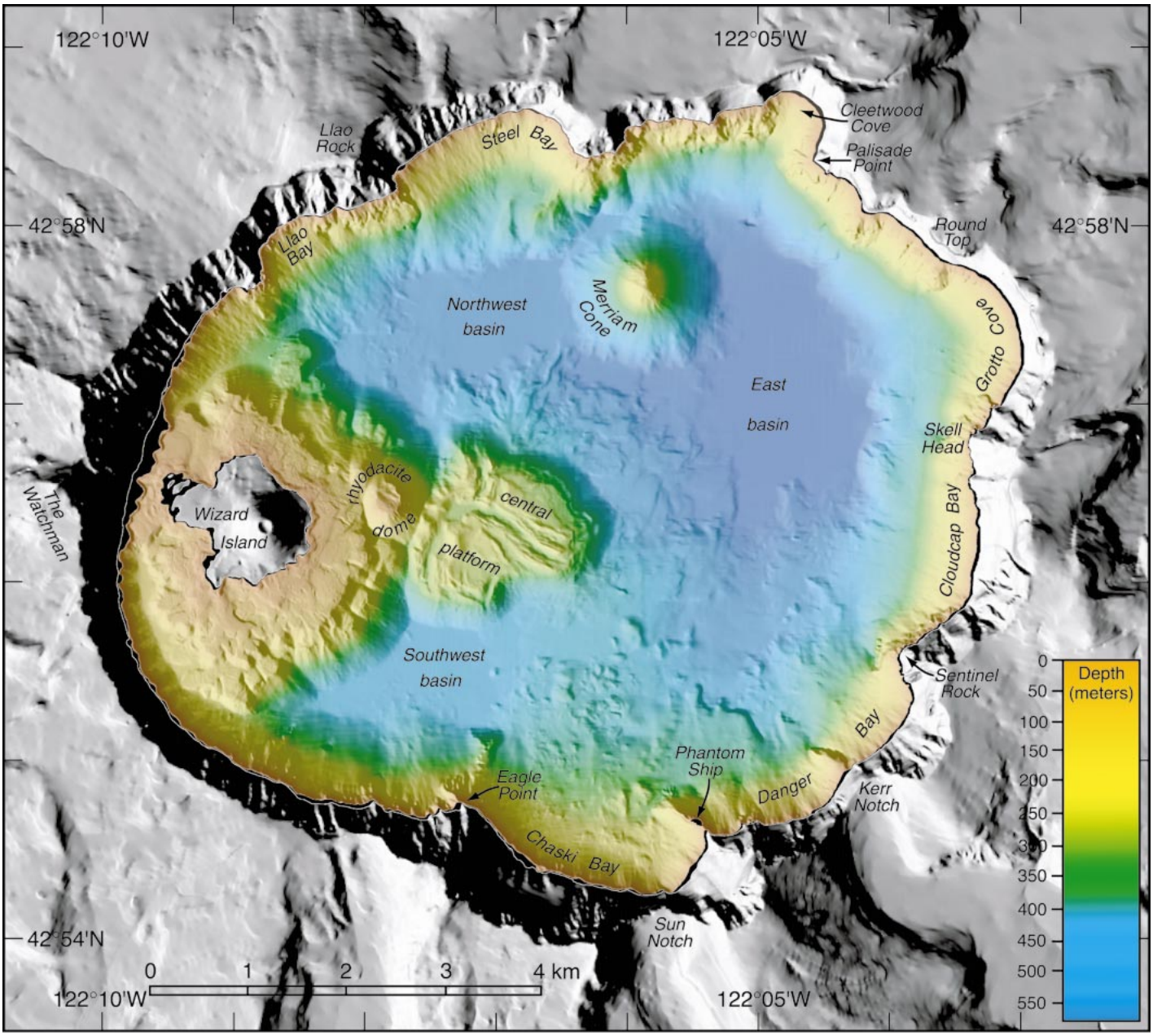

Figure. 1. Shaded relief map of the floor of Crater Lake. Surrounding terrain from USGS 10 m digital elevation model (DEM). Illuminated from 225° azimuth, 45° elevation.

footprint of 9.0 km^2, and its volume is at least 2.6 km^3 (Table 1). Beneath the surface of the lake is a broad, shallow lava flow field that is continuous with the lava flows of Wizard Island and has a range of backscatter intensities that are higher on the north and west and lower on the south and east, possibly reflecting terrigenous sediment cover decreasing to the southeast (Fig. 2). On the west side of the island, lava abuts the caldera wall 1.5 km from the vent, and the rubbly flow surface is buckled into convex-west arcuate ridges. Here, active talus of the caldera wall has built out into Crater Lake over the lava. Elsewhere around Wizard Island, at 0.9–1.5 km from its source vent, the lava drops abruptly in a surface generally sloping at 29°–36° that has relatively high backscatter (–22 dB), interrupted by gently sloping, lower-backscatter (–24 to −34 dB) benches that are comparatively shallow on the southeast and deep on the north (Figs. 2 and 3).

The morphology of the Wizard Island volcano (Figs. 4 and 5) and information from two *Deep Rover* traverses form the basis of a general model for the postcaldera andesitic volcanoes. The key observations, modified after Nelson et al. (1994), are as follows: (1) the shallow bench around the island is composed of drowned subaerial lava flows, sloping at 2°–10°, that end abruptly at an elevation of ~1805 m (78 m depth); (2) the flanks below slope at 29°–36° and mainly consist of glassy, angular lava fragments and, locally, pillow-like forms; and (3) lava samples collected with the submersible are similar in composition to the contiguous Wizard Island subaerial flows and have low whole-

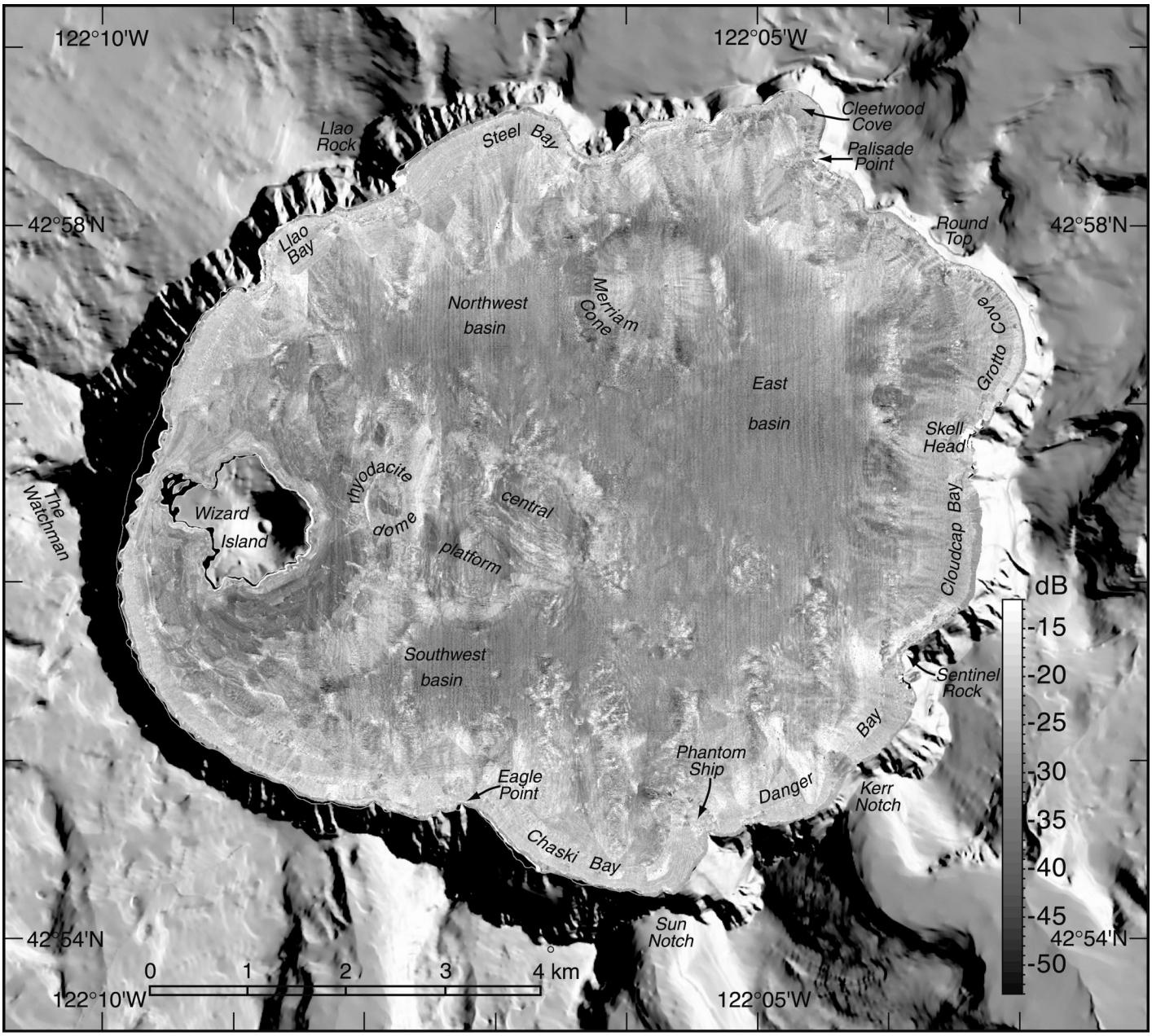

Figure 2. Acoustic backscatter map of Crater Lake. Surrounding terrain from USGS 10 m DEM. Illuminated from 225° azimuth, 45° elevation.

rock volatile (H_2O, Cl, and F) contents that imply subaerial or shallow-water eruption. The lobate terminations of the drowned subaerial lava flows and the crudely circular form of the lava field resemble historic lava flows that have entered water, as in the basaltic eruptions of Surtsey (Thorarinsson, 1967), trachytic Volcan Barcena (Richards, 1959), and dacitic Nea Kameni Island at Santorini (Fytikas et al., 1990). Upon contacting water, lava streams commonly turn abruptly, producing lobate flow terminations and a broad fan of lava flows. Chilling of lava in water results in characteristic fracturing (pseudo–pillow structures—Yamagishi [1991]; broken pillow breccias—Carlisle [1963]; pillow-fragment breccias—Staudigel and Schmincke [1984]), with the debris forming a bedded deposit whose slope may be influenced by the amount of coherent lava within the ensuing breccia. Growth of the lava field results in ''topset'' lava advancing over earlier-formed foreset-bedded breccia with the contact, or *passage zone* (Jones and Nelson, 1970), marking the water level. Exposures of the interiors of such eruptive units were described from the Columbia River Basalt and called lava deltas by Fuller (1931). The overall edifice has an internal structure like that of a tuya (Mathews, 1947), or Icelandic table mountain, formed in an intraglacial lake. Byers (1959) described two postcaldera basaltic volcanoes with tuya-like structure within Okmok caldera, Alaska, and showed that the consistent elevation of the transition from pillow breccia to subaerial lava records a former lake level. If the water level increases during a sequence of eruptions, new foreset breccia, capped by its own topset lava, may build over older topset lava (Fig. 6). Locally, particularly vigorous lava streams may survive entry into

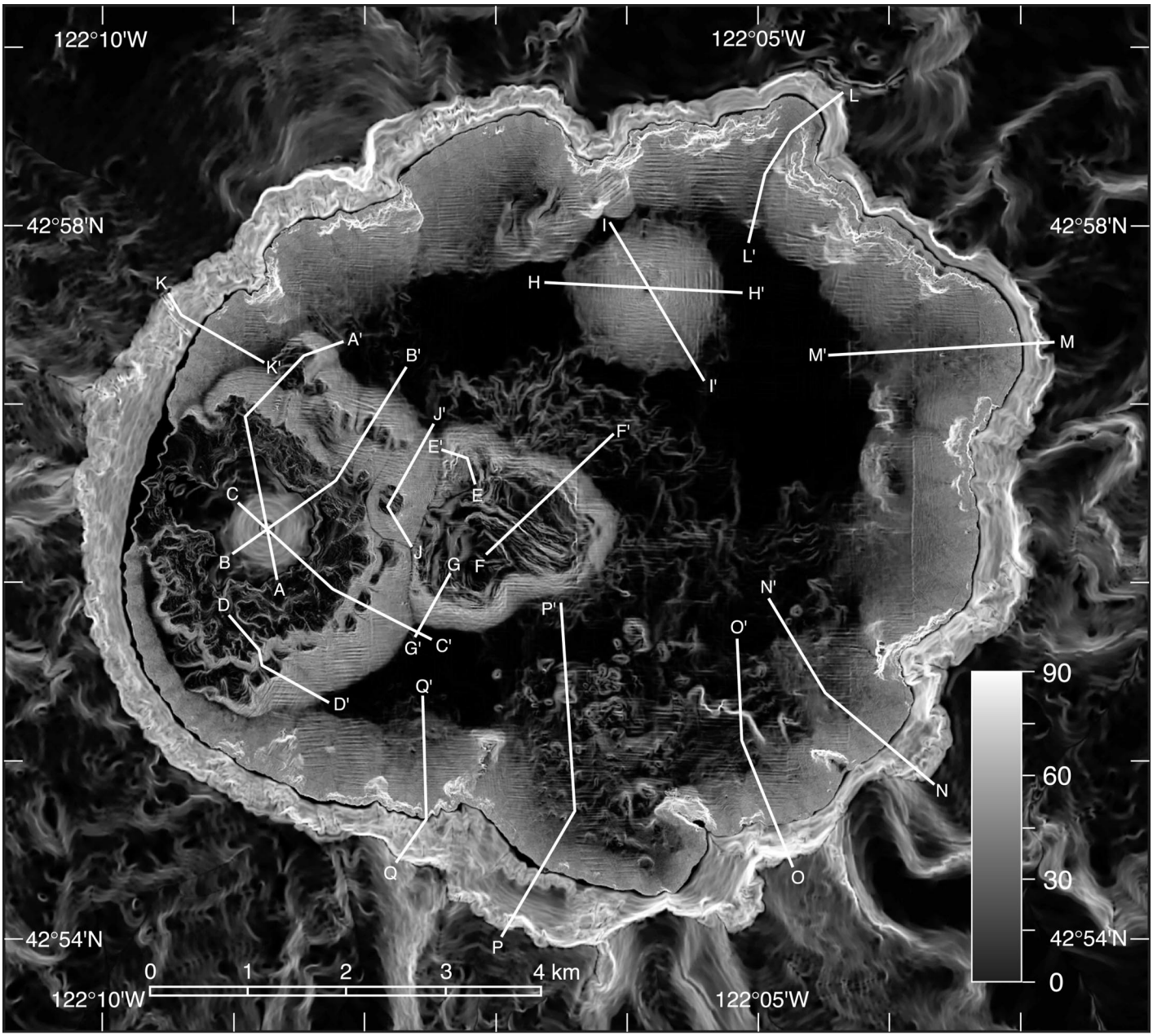

Figure 3. Slope map of Crater Lake and surrounding terrain (from USGS 10 m DEM). Brightness is proportional to steepness of slope. White lines (A–A′, etc.) indicate locations of profiles in Figures 5 and 9.

the lake (e.g., Macdonald, 1954, p. 166) and cascade down the breccia surface as coherent flows with slopes locally as steep as 45°, such as on the southeast of the Wizard Island volcano where the 1700 m bench is interrupted and on the northeast where prominent ribs mark flows that descend the slope (Fig. 7). Pillow-fragment breccia of the delta foresets probably moves farther down the slope in gravity flows to be deposited as finer-grained sediment in the deep basins of the lake. Wizard Island, then, records eruptions during the filling of Crater Lake wherein lava deltas formed several times. Of those not buried by later, more extensive deltas, the benches on the north that terminate at 1540–1560 m and 1600 m (Figs. 4, 5, and 6) preserve passage zones from early in the lake's history. The extensive bench on the southeast that terminates at ~1700 m, a full 2 km from the lava source, is a younger passage zone, as is the highest break in slope at ~1805 m. Preservation of successive passage zones implies changes in source-vent locations or decreasing eruption rates in comparison to lake-level rise. That each passage zone varies somewhat in depth is consistent with slow growth of the lava flow field and subtle differences in time of emplacement from lobe to lobe. The passage zones thus give an excellent relative chronology of postcaldera andesitic eruptions at Crater Lake.

Central-Platform Volcano

The informally named central platform (Bacon and Druitt, 1988) has a comparatively flat upper surface broken by low ridges and hills,

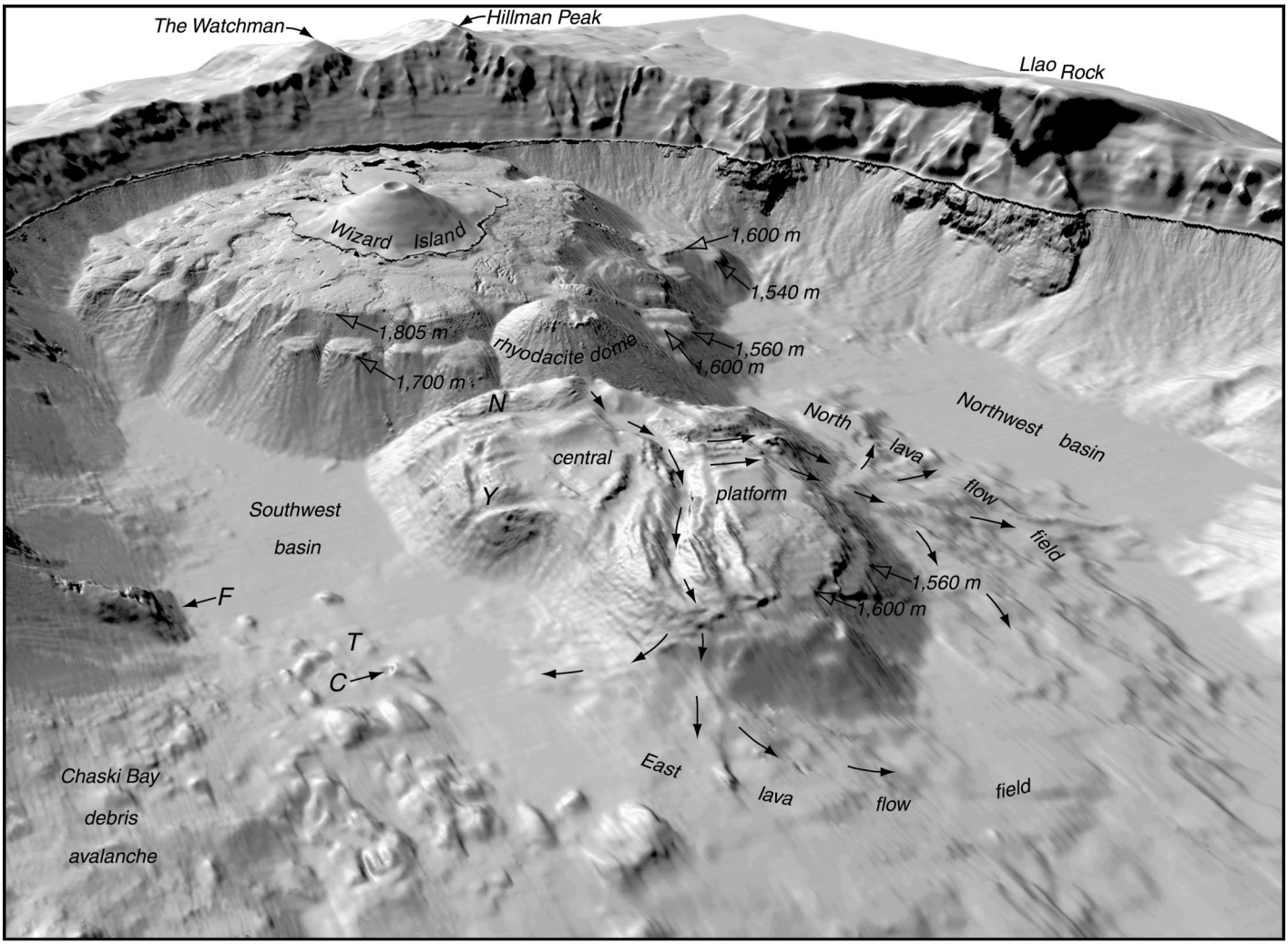

Figure 4. Perspective view of Wizard Island and central-platform volcanoes. The Wizard Island and central-platform edifices are composed of sequences of lava deltas that record past lake levels. Open arrows point to passage zones at indicated elevations where subaerial lava entered the lake and fragmented, recording former lake levels during growth of these volcanoes. Lava flowing in prominent channels on the surface of the central platform cascaded down the edifice and fed extensive subaqueous lava fields (filled arrows). These andesitic volcanoes date from the first few hundred years after caldera formation, as the lake was filling at ca. 7700–7200 cal. yr B.P. The rhyodacite dome was emplaced at ca. 4800 cal. yr B.P. East-facing scarp on central platform (*N*) may be normal-fault scarp; declivity (*Y*) probably is channel plugged by lava flow. Crater-like depression (*C*) on south side of block in Chaski Bay debris-avalanche deposit may be a collapse pit or hydrothermal explosion crater. Thermal area characterized by bacterial mats (*T*) was explored in 1988 with submersible *Deep Rover* (Dymond and Collier, 1989; Collier et al., 1991). Steep face of deep bedrock outcrop (*F*) may be remnant footwall of ring-fracture system along which cauldron block subsided during climactic eruption of Mount Mazama. Surrounding terrain appears smoother than lake floor because of poorer resolution of USGS 10 m DEM in comparison to new bathymetry. No vertical exaggeration.

flanks of nearly uniform 30°–37° slope, and more gently sloping aprons at its north and east base (Figs. 1, 3, 4, and 5). Samples collected by dredging and with *Deep Rover* consist of andesite lava similar to that of Merriam Cone and Wizard Island; those samples from the northern central platform are silicic andesites more differentiated and potassic than any other postcaldera andesite (Nelson et al., 1994). Common reddish oxidized surfaces of central-platform samples led Nelson et al. (1994) to speculate that this volcano was entirely subaerial. We consider, however, that the central platform has a history similar to that of the Wizard Island volcano. The uniformly sloping flanks appear to be foresets of pillow-fragment or angular-fragment breccia (Yamagishi, 1991) that commonly are draped in their upper reaches by more coherent lava (Fig. 7). The central platform differs from the Wizard Island volcano in the relief on its upper surface and in the presence of extensive lava fields in the deep water around much of its base. The new bathymetry shows that the sinuous flows beyond the volcano's base on the north and east can be traced up slope into prominent lava channels or collapsed tubes on top of the central platform (Fig. 4 and unpublished high-resolution views). Thus, these flows are younger, not older, than much of the central-platform edifice and, therefore, must have flowed under water. The deep flows have surface slopes of as little as 3°, margins and fronts that slope 16°, and transitional reaches that typ-

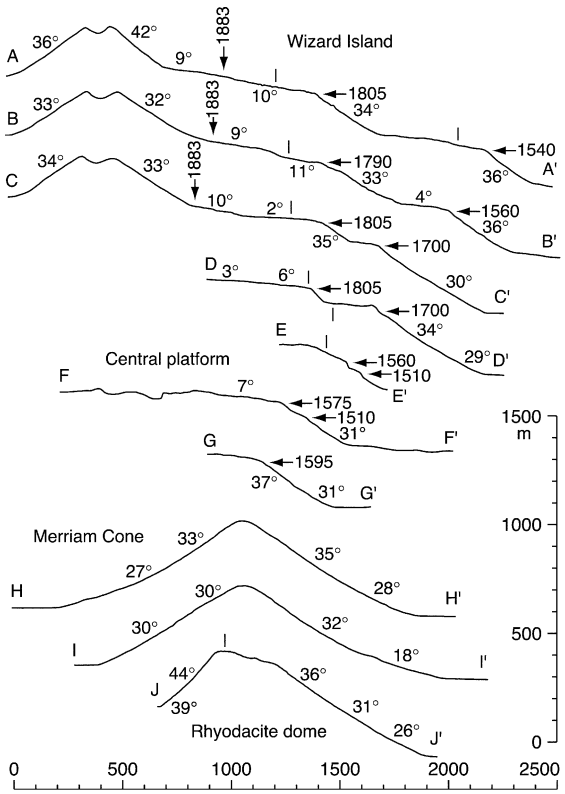

Figure 5. Representative profiles of postcaldera volcanoes. Horizontal arrows mark passage zones at indicated elevations. Vertical "1883" arrows indicate present shoreline on Wizard Island at 1883 m elevation. Vertical lines indicate change in line of profile. Measured slopes denoted by numbers with degree symbols. Subaerial lava "topsets" have gentle slopes; subaqueous "foreset" breccias have slopes near angle of repose. See Figure 3 for locations of profiles. No vertical exaggeration. Scales have arbitrary origins; vertical scale does not represent elevation above sea level.

ically slope 16° connecting the deep flows with the channels on top of the central platform. Individual flows in the north field reach 1.5 km from the central-platform edifice, and those in the east field extend 2.0 km before becoming buried by sediment. Flows may be as high as 25 m and as narrow as 75 m at the base. The backscatter intensity of deep-flow surfaces appears similar to submerged lava flows of Wizard Island and the top of the central platform, whereas the backscatter of their margins resembles breccia slopes (–22 dB). The central-platform edifice has a footprint of 3.2 km^2 and a volume of 0.76 km^3; those of the adjacent deep-flow fields are 4.9 km^2 and at least 0.30 km^3 (Table 1).

Prominent on the surface of the central platform is the east-southeast–trending lava channel that feeds the east deep-flow field. Two, and possibly three, pairs of linear ridges thought to be levees parallel the channel. The levees have higher backscatter (–16 to −19 dB) than the channel floor (–32 dB), suggesting blocky surfaces of the levees and a smooth floor. At the margins of the 30–40-m-deep, >100-m-wide channel, below the inner levees, are benches (visible on 1:15 000-scale map of Gardner et al., 2001) that probably represent flow-surface remnants left by draining of lava in the channel or collapse of a lava-tube roof. Axial symmetry of the levee system suggests widening by lateral spreading. The channel heads on the west in an apparent crater ~150 m in diameter and 35 m deep, where the central platform is onlapped by talus from the adjacent, younger rhyodacite dome. The total flow distance from the crater to the distal end of the eastern lava flows is nearly 4 km. Two similar but shorter lava channels lead to the flow field at the north base of the central platform (Figs. 4 and 7). The north-northwest channel, which curves westward downslope, may be the older, because it appears to be blocked by remnants of two levees of the main east-southeast channel (Fig. 1). The adjacent north channel, feeding the main lava field north of the central platform, appears to postdate levees, but predate the last phase of flow in the main channel. Other features of note on top of the central platform are a north-trending channel-like depression south of the crater (Fig. 4, *N*). This 35-m-deep depression is asymmetrical, its west wall sloping ~45° and the east sloping 24°. The depression appears to bend to the east at its south end and continue down the flank of the central platform, yet no lava pile or flow field is evident below it. Perhaps this feature is a normal-fault scarp local to the central platform itself. Also notable on the edifice is a Y-shaped declivity on its southeast slope (Fig. 4, *Y*) that appears to lead downslope to a small lava pile nearly covered by sediment of the southwest basin. This declivity may be a lava channel that was plugged by a sluggish, blocky flow, as suggested by the relatively high-backscatter patch at the head of the "Y."

Passage zones are evident on the central platform. The highest passage zone, at ~1600 m, defines the platform shape of the edifice and is prominent on the northeast, east, and southeast lobes. On the northeast and north-northwest flanks, discontinuous earlier passage zones are present at ~1510 m and ~1540–1560 m (Figs. 4 and 5). Passage zones at similar elevations on the north flank of the Wizard Island volcano indicate that the two volcanoes were active concurrently. We suggest that the central-platform volcano, like Wizard Island, was constructed of lava deltas, but that toward the end of its life, formation of discrete lava channels or tubes, and perhaps increased eruption rate, allowed lava to flow into the lake without fragmenting. This lava stream then descended over the platform foreset breccia to form a fan-shaped field of lava flows.

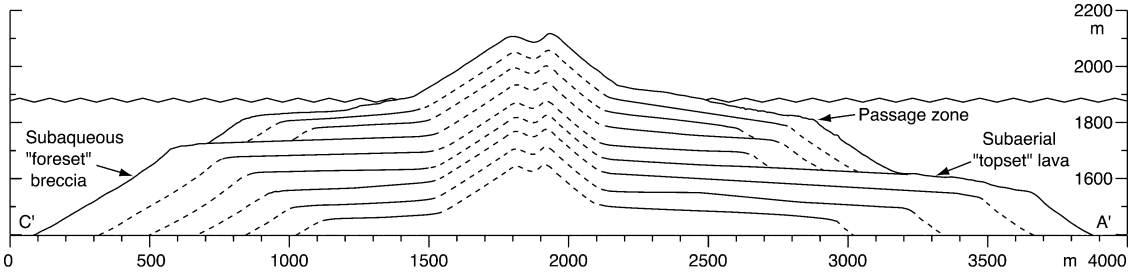

Figure 6. Schematic cross section of Wizard Island volcano after profile A′–C′ (Fig. 3), illustrating possible internal structure of edifice thought to be composed of a sequence of lava deltas formed during filling of Crater Lake. No vertical exaggeration.

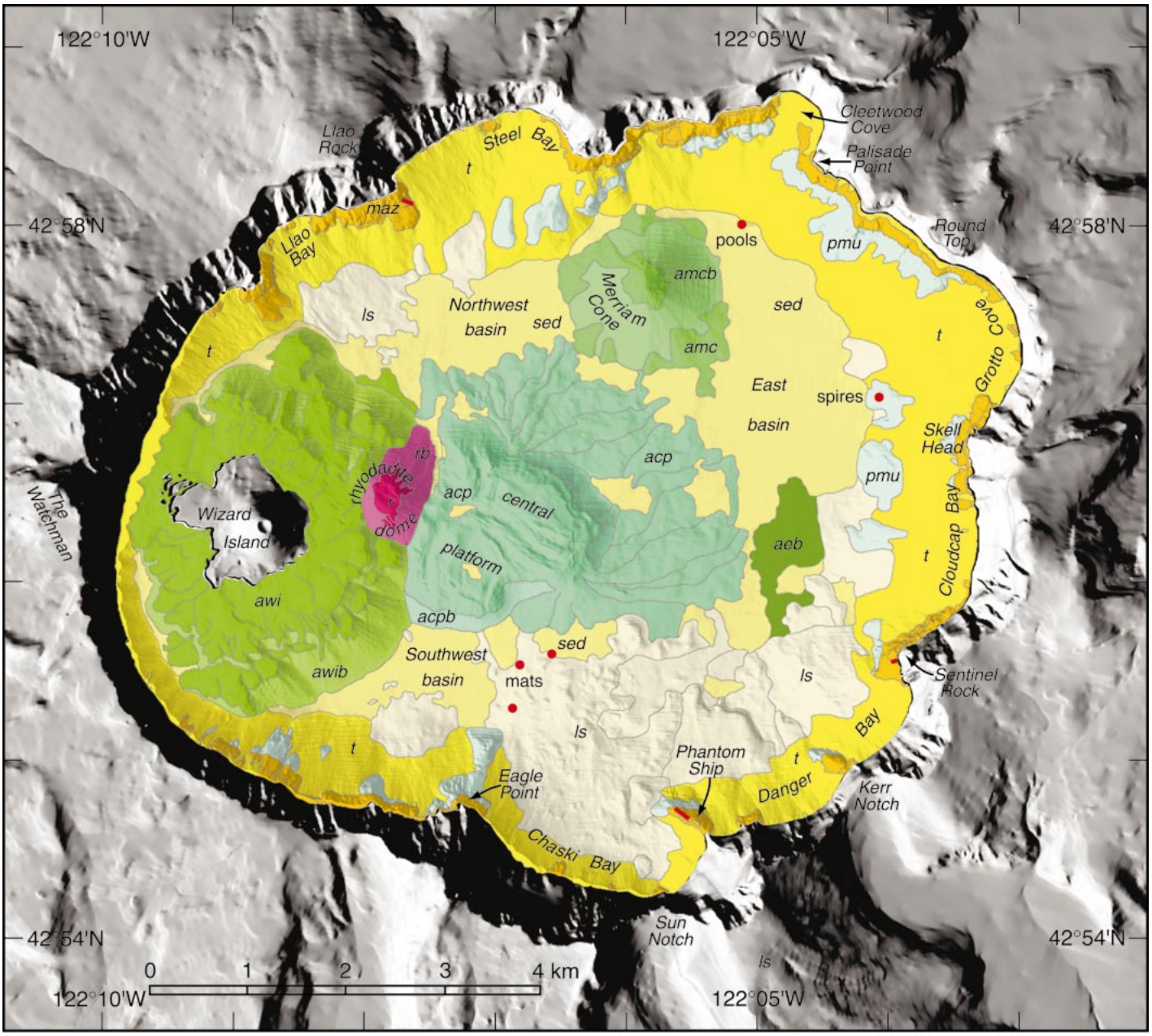

Figure 7. Generalized geologic map of the floor of Crater Lake draped on shaded relief illuminated from 225° azimuth, 45° elevation. Surrounding terrain from USGS 10 m DEM. Thermal features were discovered with submersible *Deep Rover* (Dymond and Collier, 1989; Collier et al., 1991).

Whether the vent(s) and lava channels were submerged at that time is uncertain. Because no cinder cone is preserved on the central platform, perhaps this volcano was fed by overflow or lateral dike transport of degassed magma from the Wizard Island vent or conduit.

Merriam Cone

Williams (1961) named the symmetrical hill in the north part of the lake floor Merriam Cone (Figs. 5 and 8) after J.C. Merriam, a former president of the Carnegie Institution of Washington. Its summit is 430 m above the nearby east basin, its basal diameter is 1.6 km, its footprint is 2.4 km^2, and its minimum volume is 0.34 km^3 (Table 1). Dredged andesite samples from Merriam Cone are compositionally similar to the most differentiated analyzed Wizard Island lava (Nelson et al., 1994). Radial ridges on the cone, some with lobate downhill terminations, suggest lava flows, as do buttresses near the base that slope more gently than the main cone surface and have relatively low back-

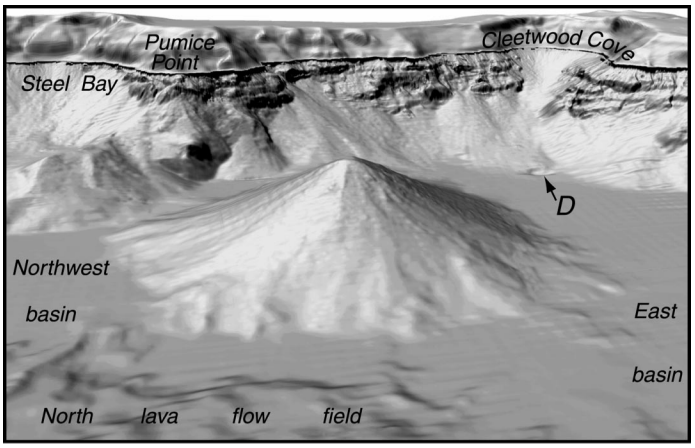

Figure 8. Perspective view of Merriam Cone and part of the north caldera wall. Andesitic Merriam Cone probably last erupted near the end of activity of the Wizard Island volcano. The surface breccias suggest that Merriam Cone erupted subaqueously. Sediment from the caldera walls accumulated in the deep basins of the lake and moved from the northwest to the deeper east basin via the low ground bounded by central-platform lava and the Merriam Cone. Depression in the caldera floor (*D*) is at the foot of a tongue of debris that descended from Cleetwood Cove. Pools of relatively warm, dense, solute-rich water were found in 1989 on the north side of the depression with submersible *Deep Rover* (Collier et al., 1991). Surrounding terrain from USGS 10 m DEM. No vertical exaggeration.

scatter intensities (Fig. 2). At the southwest and, especially, southeast base, the buttresses merge into probable lava flows that spread out onto the caldera floor (Fig. 7). Most of the surface of Merriam Cone slopes 30°–32°, decreasing to ~20° near the base (Figs. 3 and 5), has medium backscatter (–22 to −28 dB), and probably is composed of breccia similar to that on the flanks of the other postcaldera volcanoes. The uppermost fourth has an irregular surface suggestive of more coherent lava, has a small facet that slopes gently north from the summit, and lacks any hint of a crater. Williams (1961) suggested that the eruption that formed Merriam Cone was subaerial, but Nelson et al. (1994) presented evidence for subaqueous eruption. Video images from a ROV survey show fragments of prismatically jointed andesite blocks or pseudopillows and surficial fracture patterns indicative of rapid chilling of lava. Dredge samples are glassy, angular fragments, many of which are pieces of prismatically jointed blocks, that lack surface oxidation and have small vesicles, all features consistent with subaqueous eruption. Because whole-rock volatile contents are similar to those of subaerially erupted Wizard Island samples, the final Merriam Cone eruption must have occurred in shallow water. We envisage Merriam Cone as having formed in a manner similar to the Wizard Island and central-platform volcanoes, but not breaching the lake surface and forming a topset lava cap late in its eruptive history.

Other Postcaldera Andesite

A low north-trending ridge ~250 m wide protrudes 200–400 m into the south end of the east basin (unit *aeb*, Fig. 7). The ridge bifurcates at its terminus and slopes ~13° into the basin where it disappears beneath modern sediment. At least five concave-north arcuate steps several meters high and 100–200 m long on its upper surface resemble headwall scarps and have treads that slope gently to the south, as though the surface broke up during flow northward. The ridge has an overall northward slope of 1°–2° where not affected by the steps. With relatively high backscatter (up to −15 dB, Fig. 2), this ridge may be sediment-covered lava, presumably andesite. The same material apparently continues ~300 m to the west, south of the east basin, where it appears to be overlain by andesite of the central platform (Fig. 7 and unpublished detailed views). The volume of this probable lava is at least 0.032 km^3. A narrower, Z-shaped ridge to the south also has low backscatter and may be either lava or a series of large slide blocks. If any of these features is, in fact, postcaldera lava, then the source vent lies buried by younger debris-avalanche material on the south that headed between Kerr Notch and Sentinel Rock. Such a vent would be within ~500 m of the base of caldera-wall rock outcrops off Sentinel Rock. If not lava, the ridge(s) may be a secondary slide or far-traveled matrix facies of a debris-avalanche deposit that is older than the one to its south.

Rhyodacite Dome

A small hill abuts the Wizard Island volcano on its east flank (Fig. 4), reaches an elevation of 1854 m (29 m depth), and has a volume of 0.074 km^3. The approximately circular summit region forms three steps, down-to-the-northeast, separated by scarps (Fig. 1). The highest flat has low backscatter (–36 dB) (Fig. 2), consistent with its smooth, lightly striated surface observed with *Deep Rover*. Dredge samples are poorly vesiculated hornblende rhyodacite vitrophyre (Bacon and Druitt, 1988; Nelson et al., 1994). Below this lava, which forms a relatively steep flow surface that descends farther on the north than south (Fig. 7), are nearly uniform 32°–34° slopes that decrease northeastward to 26° distally (Fig. 5). These slopes have high backscatter (–16 dB) and apparently are composed of rhyodacite talus or breccia that overlies the Wizard Island and central-platform volcanoes. If we assume that the lake level has not decreased significantly since the end of Wizard Island eruptions and we consider that the highest passage zone on the Wizard Island volcano is at 1805 m, then we are led to the conclusion that much, if not all, of the dome was emplaced under water. Nelson et al. (1994) reported a radiocarbon date of 4240 ± 290 yr B.P. for sediment directly beneath a 6-cm-thick ash bed recovered in a core from the central platform and stated that the ash has phenocryst mineral compositions identical to those in the dome lava. If we accept that the radiocarbon date applies to the dome-forming event, then the calendrical date (Stuiver and Reimer, 1993) of the rhyodacite eruption is 4830 +460/–410 yr B.P.

Williams (1961) suggested that the hill is a Peléan dome. Alternatively, it may have an interior composed of breccias and lava lobes, as described by Yamagishi (1991) in eroded subaqueous silicic domes. In the latter case, the smooth upper surface and relatively steep uppermost slopes would be lava lobes and the flanks would be pseudopillows or angular-fragment breccias. The top of the dome likely owes its stepped form to slumping to the northeast, away from the Wizard Island edifice. Adjacent to the dome, northwest-trending fissures in Wizard Island lava suggest that it, too, moved northeast, possibly slumping into an explosion crater that was eventually filled by the dome.

Thermal Features

High heat flows reflecting fluid convection were measured by Williams and Von Herzen (1983) in the south and northeast parts of the lake floor. Submersible and ROV investigations of these areas revealed unequivocal evidence of modern hydrothermal circulation (Dymond and Collier, 1989; Collier et al., 1991; Wheat et al., 1998). Bacterial

mats associated with venting of warm water are present locally in the southern area near the northwest margin of the Chaski Bay debris-avalanche deposit, generally on the north side of blocks (Fig. 4, feature *T*, and Fig. 7, ''mats''; see subsequent discussion). Pools of relatively warm and solute-laden water are located at the tip of the debris tongue that descends from Cleetwood Cove to a 70 m × 220 m, 12–18-m-deep, east-trending trough (Fig. 7, ''pools,'' and Fig. 8, feature *D*). Fossil subaqueous thermal-spring deposits in the form of silica spires up to ~10–12 m high encountered by *Deep Rover* at ~550 m depth during a traverse up the caldera wall from the east basin toward Skell Head (Collier et al., 1991) apparently rise from a bedrock outcrop (Fig. 7, ''spires''). Although their locations are now placed in a geomorphic context, all of the known thermal features are too small to be resolved individually at these depths with the multibeam echo-sounder system used for the new bathymetric survey.

Caldera Walls

The new survey reveals the submerged caldera walls with sufficient detail that rock outcrops can be discriminated from fragmental material. When the central ~5 × 6 km block subsided during the climactic eruption, the unsupported walls failed by sliding, resulting in the scalloped outlines of the lake shore and caldera rim where embayments are separated by bedrock promontories. The most extensive debris slopes are in and below the deepest embayments. This is the typical mode of enlargement of the topographic, as opposed to structural, boundaries of calderas (Lipman, 1997).

Bedrock Outcrops

Detailed geologic mapping and sampling of the subaerial caldera walls (Bacon, 1983; C.R. Bacon, unpublished data, 2001) have defined sets of lava flows and pyroclastic deposits from specific vents that were emplaced during comparatively short periods in the eruptive history of Mount Mazama. Contacts between these map units commonly are expressed by benches on the caldera walls. The new bathymetric data reveal similar benches on the submerged bedrock exposures. The subaqueous bedrock exposures are lightly dusted with sediment and typically have low backscatter (–25 to −30 dB) (Fig. 2). Samples obtained in traverses with *Deep Rover* off Llao Rock, Palisade Point, Sentinel Rock, and Eagle Point enable correlation of some of these outcrops with subaerially exposed map units. In general, the deepest exposures do not have such counterparts, and most of these are shown as undivided pre-Mazama volcanic and intrusive rocks on the geologic map (unit *pmu*, Fig. 7). On the lower part of a north-trending promontory below Eagle Point, rocks mapped as *pmu* are altered to greenschist-facies assemblages and form a north-facing triangular facet that consistently dips 50° over the middle ~100 m of its ~170 m height. This face may be the footwall of a ring fault along which the central block of the caldera subsided. Five similarly deep but less rugged bluffs below Skell Head and Steel Bay mapped as *pmu* also may bound a ring-fracture system, or, alternatively, they may be massive slump blocks. Other exposures mapped as *pmu* have steeper cliffs (up to ~80°) and are likely to be in place.

Bedrock exposures can be assigned to eruptive units of Mount Mazama with confidence where they appear continuous with shoreline outcrops or where they have been sampled. Most such correlations are limited to depths of ≤150 m. Space limitations require that these be lumped as undivided lavas of Mount Mazama in Figure 7 (unit *maz*); the contact with unit *pmu* is speculative. Three dikes are large enough to be identified in the bathymetric data (Fig. 7): (1) a northwest-trending, probable andesite of Phantom Cone (Bacon, 1983, p. 68) at the top of the steep southwest-facing 80° cliff offshore of the little island called Phantom Ship (a similar dike may occur at the base of the cliff on the northeast side of this promontory); (2) a west-northwest–trending, apparent dacite of Pumice Castle (Bacon, 1983, p. 75) sampled below Llao Rock; and (3) east-northeast–trending dacite of Sentinel Rock that is continuous with the feeder for the Sentinel Rock Flow of Williams (1942).

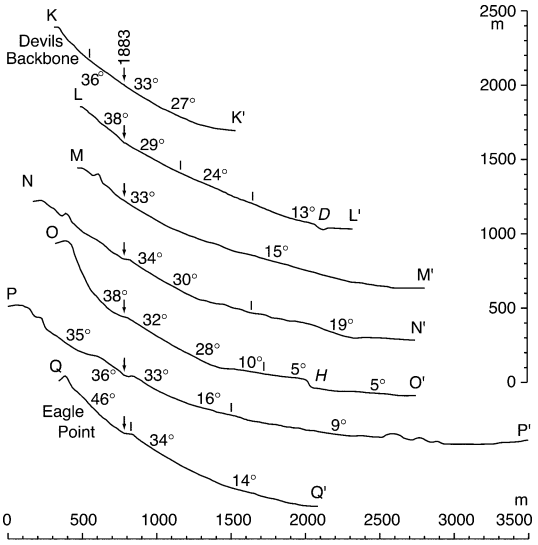

Figure 9. Representative combined topographic and bathymetric profiles of the caldera walls chosen to illustrate the slopes of fragmental materials within and below embayments. Vertical ''1883'' arrows indicate present shoreline at 1883 m elevation. Vertical lines indicate change in line of profile. Measured slopes denoted by numbers with degree symbols. Upper parts of bathymetric profiles are in talus and finer debris-apron material, whereas lower, more irregular parts of M–M′ through Q–Q′ are in debris-avalanche deposits. A secondary slide is present to the northeast of the steep headwall (*H*) in O–O′. Note prominent wave-cut platform (1877–1883 m elevation) ~50 m wide in N–N′ and Q–Q′. Data above lake level from USGS 10 m DEM. No vertical exaggeration. Scales have arbitrary origins; vertical scale does not represent elevation above sea level.

Talus, Rockfalls, and Debris Flows

Much of the submerged caldera wall is buried under fragmental debris aprons shown as talus (unit *t*) on the geologic map (Fig. 7). This unit appears to overlie or grade into landslide deposits (described subsequently). Subaerial talus of the caldera walls slopes 32°–38° where not confined by avalanche chutes or run out onto subhorizontal surfaces. The slope of subaqueous fragmental debris systematically decreases with increasing depth (Fig. 9). The higher-elevation sublacustrine slopes are 29°–35°, and the debris commonly is continuous with subaerial talus (e.g., profiles K–K′ and M–M′). Sublacustrine deposits are narrow talus cones that commonly head in bedrock debris chutes, have a longitudinally lineated or corrugated surface with a wavelength as little as 20–30 m, and are comparatively bright in backscatter (Fig. 2). The talus cones have a dendritic pattern that leads to fewer, wider ridges downslope (Fig. 10). Middle elevations are characterized by slopes of 22°–31°, a more pronounced lineation, and a variation in

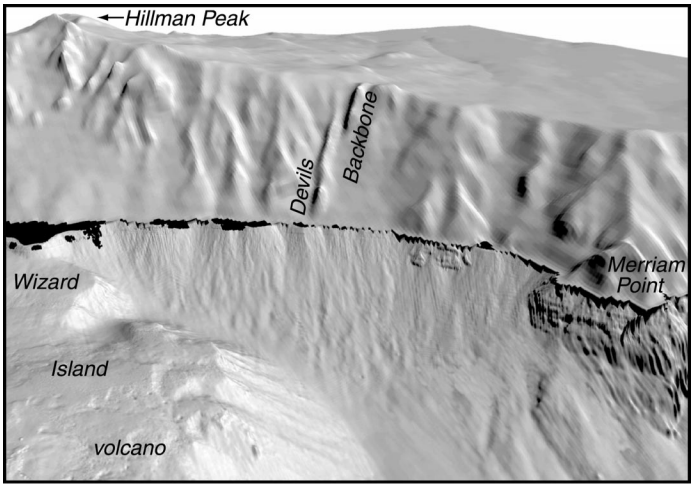

Figure 10. Perspective view of west caldera wall near Devils Backbone andesitic dike. Fragmental debris of the submerged caldera wall displays typical dendritic, lineated surface texture, with broader ridges downslope. Sediment from the caldera wall also is channeled between the Wizard Island volcano and the debris apron below Devils Backbone, ultimately into the northwest basin where it has buried much of the debris-avalanche deposit north (to right) of Merriam Point. Steeply grooved appearance of bedrock outcrops below Merriam Point is an artifact of data processing enhanced by illumination direction. Surrounding terrain from USGS 10 m DEM. No vertical exaggeration.

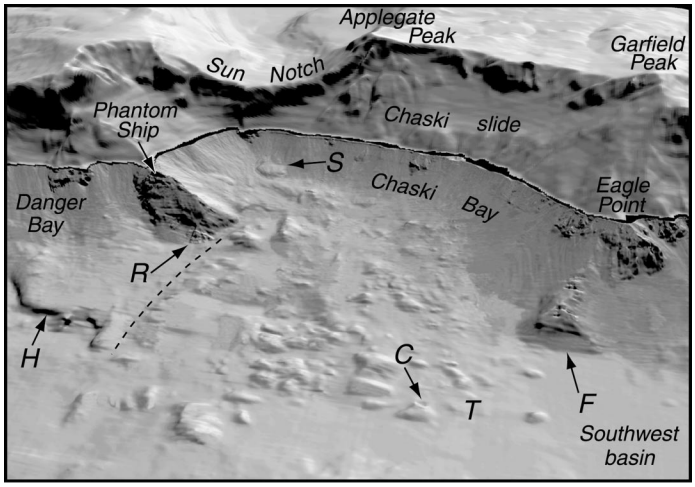

Figure 11. Perspective view of south caldera wall and Chaski Bay debris-avalanche deposit. Hummocky topography is formed by blocks derived from caldera wall surrounded by smoother matrix-facies debris. Dashed line indicates eastern limit of Chaski Bay deposit. "Chaski slide" is a slumped block of caldera-wall lavas. Crater-like depression (*C*) on south side of block in Chaski Bay debris-avalanche deposit may be a collapse pit or hydrothermal explosion crater. Thermal area characterized by bacterial mats (*T*) was discovered in 1988 with submersible *Deep Rover* (Dymond and Collier, 1989; Collier et al., 1991). Steep face of deep bedrock outcrop (*F*) may be remnant footwall of ring-fracture system along which cauldron block subsided during climactic eruption of Mount Mazama. Small rotational slump (*S*) is present below Sun Notch, a truncated glacial valley. Coarse rockfall (*R*) is preserved unburied at foot of cliff below Phantom Ship where there is no source of abundant finer clastic material. Prominent scarp below Danger Bay is headwall (*H*) of secondary slide in debris-avalanche deposit. Surrounding terrain from USGS 10 m DEM. No vertical exaggeration.

backscatter from bright to medium with a wavelength of 50–100 m. This zone may contain a transition from coalescing talus cones to more localized debris flows. In many places, this zone grades into recognizable landslide material (unit *ls*, Fig. 7), and the contact is drawn at a subtle change in slope. The lowest-elevation, or base-of-slope, deposits mapped as unit *t* have slopes of 13°–22° and abut or are buried by sediment of the basins. A continuous gradation from shoreline talus (32°) to base-of-slope mass flow (13°) can be found in Cleetwood Cove (profile L–L′), where the flowage deposit terminates with a 40° slope into a depression on the caldera floor (see Thermal Features section; Fig. 7, "pools," and Fig. 8, feature *D*). Isolated 10–30 m blocks are resolved locally in unit *t*, such as below Grotto Cove, Steel Bay, and southern Danger Bay (not visible at scale of figures). A few coarse rockfalls have been identified at the bases of steep cliffs that lack talus sources above, as at the north and east bases of the Phantom Ship promontory (Fig. 11, feature *R*). At the highest resolution in comparatively shallow water (unpublished views), bedforms are visible in sediment resting on bedrock surfaces (e.g., ~20 cm amplitude and 1.5–2.0 m wavelength, below Round Top).

Drowned Beaches, Wave-Cut Platform

A total of nine drowned beaches have been identified—and up to seven are present at a given locality—below the shore of Crater Lake wherever relatively fine, unconsolidated fragmental deposits occur. The upper beaches are visible underwater along the shore of Wizard Island (Fig. 12) and from the caldera rim at Cleetwood Cove and The Watchman. Beaches, defined as bands of nearly flat terrain parallel to the lake shore and identified by using a slope map of the bathymetric data supplemented by high-resolution profiles, have average elevations of 1848.5, 1852.5, 1855.2, 1857, 1859.5, 1860.7, 1872, 1875, and 1877.5 m. Deeper beaches have not been recognized. No systematic variations in elevation of a given beach around the lake have been detected. The shallowest drowned beach represents the deepest part of a wave-cut platform, commonly up to 40 m and rarely as much as 100 m wide, that is continuous between ~1877 and 1880 or possibly as high as 1883 m (Fig. 9) and is well documented by the bathymetric data. This platform is widest and best developed in talus and altered lavas of the west, southwest, south, and east shores (e.g., Q–Q′). It appears in Figure 1 as a black (no data) band between topographic and bathymetric coverage (note that the bathymetric survey includes the deeper parts of the platform; the wide, lobate, black area west of Wizard Island is subaerial talus).

Landslides and Debris Avalanches

Hummocky topography and scattered large blocks on the lake floor below many of the embayments in the caldera wall mark the locations of landslide and debris-avalanche deposits (Fig. 1; Table 1; unit *ls* in Fig. 7). The slide deposits present graphic evidence of caldera enlargement by mass wasting, possibly triggered by earthquake shaking. It is convenient to adopt the terms applied to volcanic debris-avalanche deposits by Crandell et al. (1984) and Glicken (1998): *Block facies* con-

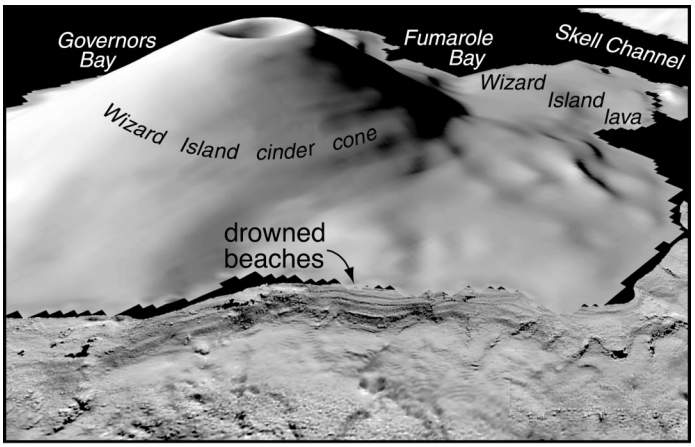

Figure 12. Perspective view of drowned beaches on northeast of Wizard Island. Beaches are thought to reflect climatically regulated stillstands at various times after lake filled rapidly to ~1850 m elevation. Slumps have modified some beaches, particularly on right half of image. Bathymetry not shown in background (black). Surrounding terrain from USGS 10 m DEM. No vertical exaggeration.

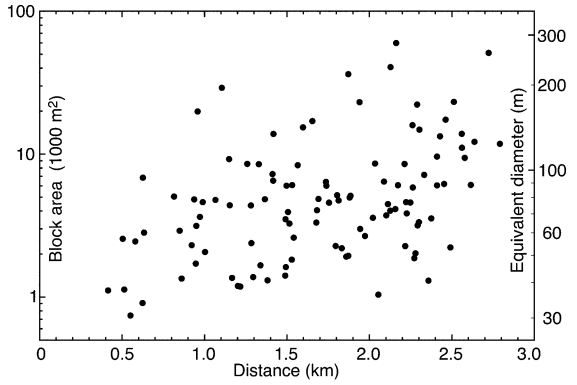

Figure 13. Plot of block size in Chaski Bay debris-avalanche deposit as a function of distance from lake-shore reference point below Sun Notch. Scale to left—areas of individual blocks; scale to right—diameters of equivalent circles. Apparent increase in block size with distance may be artifact of greater burial of blocks closer to caldera wall. Maximum travel distance was insufficient to destroy large blocks.

sist of debris-avalanche blocks that may be brecciated or unconsolidated but were transported relatively intact; *matrix facies* are unconsolidated mixtures of particles or clasts that range in size from micrometers to meters. There probably exists a continuum between matrix-facies landslide deposits that are continuous with flowage deposits of the middepth unit *t* aprons and large debris-avalanche deposits. The latter probably formed in single events and commonly are affected by secondary failures that themselves generated landslides.

Debris-Avalanche Deposits

Deposits of large debris avalanches are among the more striking morphologic features of the lake floor (Fig. 1). They strongly resemble the much larger submarine landslide deposits from volcanoes in the oceans (e.g., Moore et al., 1989; Krastel et al., 2001). The debris-avalanche deposits at Crater Lake consist of block-facies mounds immersed in low-relief, matrix-facies debris (Crandell et al., 1984; Glicken, 1998). The contrast between block tops, which commonly have low backscatter (–32 to −35 dB), and the rather variable matrix-facies and block sides results in a mottled appearance (Fig. 2). Debris-avalanche deposits are best developed below embayments in the south and southeast caldera walls within the older part of Mount Mazama. Here, near the eruptive center of early Mount Mazama, the rocks are hydrothermally altered, and the intensity of alteration increases with depth. Clay-rich, altered flow-top breccias probably acted as failure surfaces for avalanching of the original caldera walls into the subsiding caldera during the climactic eruption. Postcaldera debris avalanches probably formed in the same way. Observations and samples from dives with *Deep Rover* are consistent with mounds in the Chaski Bay debris-avalanche deposit being block-facies material composed of highly fractured rock derived from the caldera walls (Nelson et al., 1994).

The Chaski Bay debris-avalanche deposit is the largest example of its kind at Crater Lake (Fig. 11). This deposit has an area of 4.9 km^2 and a volume of at least 0.21 km^3 (Table 1). The largest blocks are ~280 m long (a possibly composite block is ~450 m long) and traveled 2–3 km from source. In this and the other Crater Lake debris avalanches, most of the large blocks tend to be found near the distal end of the deposit (Fig. 13), although secondary slides may extend farther. It is unclear to what extent the apparent increase in block size with distance is caused by draining of matrix-facies material from the distal end and burial of blocks in the proximal area. An increase in block size with distance also was reported for the subaqueous McKinney Bay debris-avalanche deposit in Lake Tahoe (Gardner et al., 2000a). Blocks in the Chaski Bay debris avalanche apparently did not travel far enough to break up so that maximum block size does not decrease with distance, in contrast to volcanic debris avalanches of comparable vertical drop that traveled 5–10 km (Siebert, 1984). Although Nelson et al. (1994) suggested that the Chaski Bay debris avalanche reached the central platform and was diverted to flow another ~2 km to the northeast, the new bathymetry indicates that this debris avalanche stopped when it apparently rode up on the south-facing slope of the lava flow field at the southeast base of the central-platform edifice. The terrain immediately east of the edifice is underlain by andesite lava from the central platform and is not composed of debris-avalanche material (Fig. 7). In this interpretation, the Chaski Bay debris avalanche would have occurred when the lake level was at least at 1600 m elevation because the underlying lava flows were emplaced after the central-platform lava delta exceeded that elevation.

Debris avalanches originating at Chaski, Danger, and Cloudcap Bays were directed toward the east basin by the underlying lava flows from the central platform or were deflected by older debris-avalanche deposits. The hummocky, high-backscatter ridge that forms the east margin of the Chaski Bay debris-avalanche deposit appears to have been deflected to the north by the apparently older, low-backscatter, smoother debris-avalanche deposit north of Phantom Ship (Fig. 11). Low-relief probable landslide debris below Cloudcap Bay appears to have been deflected northward by the low ridge to its west that projects into the east basin (Fig. 7).

Smoothed longitudinal profiles of debris-avalanche deposits extend the general parabolic form of unit *t* deposits (Fig. 9). Slopes of matrix-facies material are typically 4°–6° and locally 0°. Ratios of *H*/*L* (vertical drop to travel distance) are estimated to be ~0.2–0.5 for the various debris avalanches at Crater Lake (range reflects assumption of *H* for center of mass versus maximum *H* from caldera rim), values more

typical of subaerial nonvolcanic landslides than of volcanic debris avalanches (0.05–0.2; Ui, 1983; Siebert, 1984). Semicircular closed depressions are present on debris-avalanche deposits. Some are bounded by blocks. A circular depression ~60 m in diameter and 4 m deep bites into the southwest base of a 170-m-long block near the northwest end of the Chaski Bay debris-avalanche deposit (Figs. 4 and 11, feature *C*). This feature is suggestive of a collapse pit (cf. Glicken, 1998) or, possibly, a hydrothermal explosion crater.

Secondary landslides have formed by failure of the lower reaches of the larger debris-avalanche deposits, such as below Danger Bay and north of Phantom Ship. The secondary slide deposits have the morphology of matrix facies or comparatively fine block facies. Source-scar headwalls slope 20° to as much as 51° (Fig. 9, *H* in O–O′) for the extensive, 70-m-high scarp in the debris-avalanche deposit north of Phantom Ship (Fig. 11, *H*). A major secondary slide now occupies the channel defined by this scarp and a counterpart to the east. This mass has very high backscatter (–10 dB) within the channel, whereas the hummocky, block-facies terrain beyond the channel mouth has convex-north bands of medium and low backscatter (–20 and −32 dB, respectively) as though the bands correspond to pressure ridges in landslide debris and intervening sediment ponds. Measured slopes of surfaces of secondary slide deposits are 4°–6°; one slide has a reversed 3° slope toward the headwall. A sediment pond may partially fill a depression between the headwall and the secondary slide mass (Fig. 7).

Matrix-Facies Landslide Deposits

Examples of landslide deposits that appear to be composed largely or entirely of matrix-facies material occur west of Eagle Point and below Llao Bay, Steel Bay, and Grotto Cove (Fig. 7). Each of these is essentially continuous with the talus and/or debris apron above it (Fig. 9, M–M′). These deposits cover areas of 0.14–0.72 km^2 and have volumes of up to 0.014 km^3 (Table 1). They appear to have formed by superposition of flow lobes, and they have been mapped separately (unit *ls*) from the more uniform surface of unit *t* above them. Primary matrix-facies landslide material slopes from a maximum of 25° at the transition from unit *t* to a 3°–7° distal runout surface.

The Eagle Point and Llao Bay deposits have probable block-facies materials at their distal ends that are partially buried by sediments of the deep basins. Conceivably, mounds at the base of the Wizard Island volcano beyond each of these debris-avalanche deposits may be far-traveled blocks that outran the main debris avalanche (cf. Prior et al., 1982). Both debris-avalanche deposits occur directly below corresponding embayments in the caldera wall.

A small slump is prominent on the upper submerged caldera wall southwest of Phantom Ship (Fig. 11, *S*). This feature has a concave source scar that slopes from ~23° down to a 4° tread and deeper into a convex welt that slopes up to 37° at its base. It appears to have formed by motion of a coherent mass of debris ~180 m across and ~30 m thick over a distance of ~100 m.

Sediment Ponds and Basins

The three major basins of the lake floor and numerous smaller depressions on and between lava flows and landslide deposits have smooth, nearly flat surfaces with uniformly low backscatter (–32 dB; Fig. 7, unit *sed*).

Basins

The east, northwest, and southwest basins are the main repositories of fine clastic sediment. Nelson et al. (1986) described gravity cores and seismic reflection profiles from the base-of-slope aprons (units *t* and *ls*) and the basins. They proposed that sediment gravity flows transported debris to the base of the caldera-wall slope where it was deposited as thick, coarse-grained layers on the aprons. The finer-grained part continued into the basins as sheet-flow turbidity currents that deposited fine-grained, well-sorted, and graded sand layers.

The sand/mud ratios in the upper 8 m of lake sediments decrease with distance from the wall. Backscatter values determined in the new survey tend to be lower farthest from clastic sediment sources; this trend may reflect the reported decrease in sand-sized sediment with distance. From seismic reflection profiling, Nelson et al. (1986) gave maximum sediment thicknesses as 75 m in the east basin and <50 m in the southwest and northwest basins. Nelson et al. (1988) suggested that the lower part of the sediment in the basins is nonlacustrine material deposited rapidly after the caldera formed.

Sediment Ponds and Sediment-Flow Patterns

The new survey reveals many flat, low-backscatter, sediment-filled areas apart from the three main basins and delineates sediment-transport paths along the lake floor. The main channels formed by the Wizard Island edifice and the adjacent caldera wall funnel sediment to the southwest and northwest basins while filling local depressions along these pathways. Similar processes occur between Merriam Cone and the caldera wall. Local sediment ponds occur on the central platform and its apron of lava flows, including many that are too small to illustrate in Figure 7. Sediment also fills depressions where debris-avalanche deposits terminate against central-platform lavas, below headwall scarps of secondary slides (e.g., north of Phantom Ship), and between Merriam Cone and the central-platform lava flow field. The northwest basin and many of these sediment ponds are dammed by low ridges (sills), and sediment can be envisaged as moving through the ponds to ultimate sinks in the southwest and east basins.

DISCUSSION

Collapse of the Caldera

The new survey improves our knowledge of the deep caldera walls and the structure of Crater Lake caldera. The mode of collapse of calderas the size of Crater Lake and smaller continues to be controversial, whether by chaotic or piecemeal subsidence, funnel-shaped collapse into a central vent, or subsidence of a coherent block along ring fractures (Lipman, 1997). The steep underwater cliff deep below Eagle Point (Fig. 4, feature *F*) may be a remnant of a ring-fracture footwall. Other apparent bedrock exposures deep below the east and north walls must be close to the structural boundary of the subsided caldera floor. Merriam Cone and Wizard Island are thought to mark ring-fracture–controlled vents (e.g., Nelson et al., 1994). The 2000 survey points to a third volcanic vent (for unit *aeb*, Fig. 7) obscured by younger debris and located below the southeast caldera wall, coincident with the likely ring-fracture zone. Similarly, all known thermal features occur near this zone (Fig. 7; Williams and Von Herzen, 1983; Dymond and Collier, 1989; Collier et al., 1991). The rhyodacite dome and central-platform vents, although inboard of the proposed ring-fracture zone, are nonetheless west of the caldera center. The debris-avalanche deposits and scalloped topographic form of the caldera walls clearly show that the caldera was enlarged by caving and sliding of its original walls into the structural depression. These observations are consistent with physical volcanological evidence (Bacon, 1983; Druitt and Bacon, 1986;

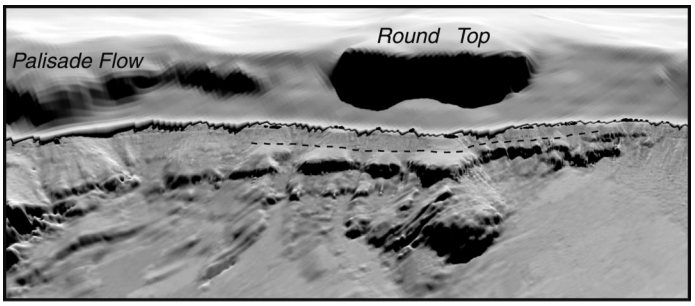

Figure 14. Perspective view of northeast caldera wall near Round Top. Andesite of Round Top (ca. 160 ka) rests on unconsolidated, fragmental deposits, which are largely hidden underneath modern talus and pinch out to the northwest (left) beneath the younger, dacitic Palisade Flow. Dashed line marks base of this permeable layer where it lies on glaciated lava surface. This interface is the lowest known horizon where a marked permeability contrast appears to occur. Seepage through the fragmental layer evidently prevents Crater Lake from filling to levels more than a few meters higher than present elevation of ~1883 m. Appearance of linear ridges inclined to left in lower part of image is an artifact of data processing enhanced by illumination direction. Surrounding terrain from USGS 10 m DEM. No vertical exaggeration.

Suzuki-Kamata et al., 1993) for ring-fracture subsidence of Crater Lake caldera.

Filling of Crater Lake

The level of Crater Lake is maintained by input from precipitation and losses by evaporation and seepage (Phillips, 1968; Redmond, 1990; Nathenson, 1992). The principal unknown in this balance is the nature of the seepage. Bacon and Lanphere (1990, p. 26) pointed out that the caldera floor and the walls below the lake surface are likely to have low permeability owing to hydrothermal sealing of fractures and breccias and that lake level may be controlled by relatively permeable fragmental deposits at water level in the northeast part of the caldera. The lava surface upon which these deposits rest at elevations of ~1844–1859 m is evident in the new bathymetry (Fig. 14). If current precipitation and evaporation rates are assumed in conjunction with no seepage loss, Crater Lake would fill to the permeable horizon at ~1844 m in as little as 250 yr (model 1), but models for filling under the warmer, drier conditions of ~70% of current precipitation (model 2) indicated by paleoclimatic reconstructions (e.g., pollen record in Nelson et al., 1994) yield ~650 yr (Nathenson et al., 2001). These models do not take into account the unknown initial hydrologic conditions related to caldera collapse such as inflow of groundwater from the caldera walls and higher evaporation rate.

The drowned beaches (Fig. 12) may record climatically regulated stillstands of Crater Lake that were possible once the permeable horizon was reached; note that the deepest submerged beach recognized has an elevation of 1848.5 m. The level of Crater Lake has fluctuated ~5 m during the past century (Redmond, 1990). A lowstand of Crater Lake in the 1930s and early 1940s (Redmond, 1990, Fig. 1; average ~1878.7 m) corresponds to the deepest part of the wave-cut platform. Lichen growth lines and old-growth forest close to present lake level and absence of old shorelines on Wizard Island and elsewhere suggest that the lake has not been significantly higher in the past (Nelson et al., 1994). However, Peterson et al. (1999) reported that only trees <150 yr old are found along the lower wall of the caldera and shoreline of Wizard Island. Their model for lake-level variation since A.D. 1687 based on dendrochronology of *Tsuga mertensiana* suggests a maximum of ≥9 m higher than recent low levels, or ~1888 m. It is possible that Crater Lake has risen and fallen between 1849 m and at least 1883 m many times in response to climate (cf. Stine, 1990) since the permeable horizon was first encountered during lake filling. However, the impressive wave-cut platform at 1877–1883 m (Fig. 9) argues for long-term stability of the lake surface. The passage zone at 1805 m indicates that the lake surface was at that elevation at the end of lava effusion from the Wizard Island volcano. As discussed next, the timing of filling of Crater Lake is intimately tied to postcaldera eruptive history.

Postcaldera Geologic History

Knowledge of the geologic history of Crater Lake caldera has been expanded by mapping geologic units defined by the bathymetry, supplemented by backscatter data, results of earlier dredging, coring, seismic reflection surveying, and observation and sampling with submersible vehicles (Nelson et al., 1994). The postcaldera history proposed here is given an absolute chronology from a model for filling of the lake (Nathenson et al., 2001), on the basis of the assumption that lake water began to accumulate within a few years of caldera formation.

At the conclusion of the climactic eruption, the caldera would have contained at least 1 km of hot fill consisting of juvenile pyroclasts accumulated as the caldera subsided and intercalated breccias derived from the caldera walls as they failed inward (Hildreth, 1996; Lipman, 1997). Exposure of the hydrothermal system within Mount Mazama and inrush of groundwater from the freshly exposed caldera walls probably resulted in explosive disruption of the uppermost caldera fill. Nelson et al. (1988) mapped closed depressions in the ''acoustic basement'' surface beneath modern sediment and proposed that these are secondary explosion craters. Nelson et al. (1988) also suggested that the earliest postcaldera sediments that fill the depressions and thicken toward the caldera walls are subaerial deposits of mass-wasting processes and that the overlying basin sediments are lacustrine hemipelagic and turbidite deposits.

The inception of postcaldera volcanism is difficult to pinpoint, but apparently it closely followed caldera collapse. In addition to ejection of ~50 km^3 of magma, the climactic eruption was accompanied by collapse of the ~4000-m-elevation Mount Mazama and formation of Crater Lake caldera, removing at least 3 km of overburden equivalent to >60 MPa pressure on the magmatic system. Postcaldera andesitic volcanism reflects progress of the magmatic system toward stability following this abrupt change in mass, volatiles, and confining pressure. The northernmost Wizard Island lava delta and a similar passage zone on the northeast flank of the central-platform edifice at ~1550 m elevation are the oldest features that can be tied to a lake level and thus to a specific model time. They were followed rapidly by construction of the rest of the northern Wizard Island lava deltas and central-platform edifice to ~1600 m, showing that both vents were vigorously active concurrently when lake depth was ≤320 m (allowing for subsequent basin sedimentation). Probably at the same time, or even earlier, because lavas of the eastern central-platform flow field appear to be deflected by it, the probable lava flow that projects into the east basin effused from a vent near the southeast caldera wall. Relationships on the surface of the central platform indicate that the northern deep-flow field developed before the eastern one and suggest that effusion of the eastern lavas occurred during the last eruption of the central-

TABLE 2. MINIMUM ERUPTION RATES OF POSTCALDERA VOLCANOES

Feature	Volume (km^3)	Estimated lake elevation at time of feature's eruption (m)	Model 1 time after caldera collapse (yr)	Model 1 elapsed time (yr)	Model 1 minimum eruption rate		Model 2 time after caldera collapse (yr)	Model 2 elapsed time (yr)	Model 2 minimum eruption rate	
					Volume (10^6 m^3/yr)	Mass (kg/s)*			Volume (10^6 m^3/yr)	Mass (kg/s)*
Wizard Island N deep passage zone (below 1550 m elevation)	0.741	1550	53	53	14.0	980	89	89	8.3	580
Wizard Island SE lower passage zone (1550–1700 m elevation)	1.064	1700	131	79	13.5	940	254	165	6.4	450
Wizard Island shallowest passage zone (1700–1805 m elevation)	0.817	1805	215	83	9.8	690	489	235	3.5	240
Total Wizard Island	2.620	1805	215	215	12.2	850	489	489	5.4	370
Merriam Cone	0.342	>1732	>155	N.D.	N.D.	N.D.	>310	N.D.	N.D.	N.D.
Central platform edifice	0.758	1600	75	75	10.1	700	130	130	5.8	410
Central platform flow fields	0.300	>1600	>75	N.D.	N.D.	N.D.	>130	N.D.	N.D.	N.D.
Total postcaldera andesite	4.020	1805	215	215	18.7	1300	489	489	8.2	570

Note: Model 1: Time for lake filling assuming modern precipitation and evaporation rates. Leakage at any given lake level is taken to be proportional to lake level from total depth, plus an additional contribution (55%) that is proportional to lake level in excess of 555 m (equivalent to 1844 m basal elevation of permeable horizon (Nathenson et al., 2001). Model 2: Same as model 1 but with 70% of modern precipitation (Nathenson et al., 2001). N.D.—not determined.

*Assumes bulk density = 2200 kg/m^3.

platform volcano. The Wizard Island volcano continued to vent andesite, probably after cessation of central-platform activity, forming a prominent lava delta preserved on the southeast flank at ~1700 m and finally ceasing when the lake reached ~1805 m. Merriam Cone was constructed at an uncertain time because its entire surface appears to have been emplaced subaqueously. Similar composition for Merriam Cone and Wizard Island andesite and its low whole-rock volatile content suggesting effusion in shallow water imply final activity when the lake was at >1720 m, or a model 2 (i.e., based on 70% of modern precipitation) age of >300 yr after caldera collapse (Table 2). The entire 4.0 km^3 of postcaldera andesite evidently was vented in ~500 yr, or by ca. 7200 cal. yr B.P. By this time, >500 m of water had accumulated in the caldera, adding ≥5 MPa confining pressure to the magmatic system and possibly contributing to the pause in andesitic volcanism. The 0.074 km^3 rhyodacite dome was emplaced ~2400 yr later at ca. 4800 cal. yr B.P. Although there is no indication of volcanism after emplacement of the dome, it would be unwise to assume that there will not be future eruptions, as Mazama has been a volcanic focus for >400 000 yr (Bacon et al., 1997).

Debris-avalanche deposits were emplaced after much or all of the andesitic postcaldera eruptive period. The Chaski Bay debris avalanche appears to have run up onto lava of the central-platform east flow field, indicating that the lake was at least 320 m deep when this debris avalanche took place. Similarly, the Llao Bay debris avalanche appears to have been deflected by the north base of the Wizard Island edifice and the eastern Danger Bay debris avalanche by the lava south of the east basin (Fig. 7). Basin sediment buries the distal parts of the Lao Bay and Eagle Point debris-avalanche deposits, and sediment ponds have formed between the Chaski Bay debris-avalanche deposit and the central platform, indicating that considerable time has elapsed since the debris avalanches occurred. The Chaski Bay debris avalanche itself apparently flowed against the western Danger Bay debris-avalanche deposit north of Phantom Ship; the older debris-avalanche deposit conceivably may have been subaerial. Secondary landslides that affected it and the Chaski Bay debris-avalanche deposit clearly were subaqueous. Some or all of these slides may have been initiated by ground shaking during local $M \approx 7$ earthquakes on the West Klamath Lake fault zone or distant $M > 8$ earthquakes of the Cascadia subduction zone (Bacon et al., 1997). Alternatively, slides may have occurred during late postcaldera volcanism, such as the eruption that ended in emplacement of the rhyodacite dome (Nelson et al., 1994).

The youngest sedimentary units at Crater Lake are the gravity-flow deposits of unit *sed* that fill the deep basins and local sediment ponds and the talus and/or debris aprons that constitute unit *t* (Fig. 7). Beneath the modern surface, these must include materials that date from the early history of the caldera. The youngest material in unit *t* is continuous with unconsolidated talus and scree of the subaerial caldera walls. The morphology of the debris aprons revealed by the new survey indicates that only modest amounts of sediment reside in them or have been delivered to the caldera-floor basins since the time of major debris avalanching. This finding is consistent with earlier conclusions that, although rockfalls and debris transport are ongoing (e.g., Nelson et al., 1986), the caldera walls have been little modified since caldera formation (Bacon, 1983).

Eruption Rates

The chronology provided by the interplay between volcanism and lake filling, coupled with accurate volume determinations, allows minimum eruption rates to be obtained for the postcaldera andesitic volcanoes (Table 2). Long-term eruption rates are calculated for volumes bounded by surfaces at elevations defined by passage zones and equated with specific times based on lake-filling model 2 (70% of modern precipitation). Growth of the Wizard Island volcano is divided into three periods by prominent passage zones at ~1550 and 1700 m. Volumes of sectors of the volcano where a bounding passage zone is not exposed (e.g., between 1550 and 1700 m on the southeast flank) may be overestimated because the geometry of the lava and breccia pile erupted during that period is uncertain.

We obtain minimum-volume eruption rates of 6.5 and 3.5×10^6 m^3/yr for the middle (1550–1700 m lake level) and late (above 1700 m) eruptive periods of the Wizard Island volcano, respectively. Recognizing that estimating the form of the base of the Wizard Island edifice is prone to error, the minimum eruption rate for the early period (below 1550 m) is 8.3×10^6 m^3/yr. These results suggest a secular decrease in eruption rate for the Wizard Island volcano, as implied by failure of younger lava deltas to completely bury older ones. The central-platform edifice yields a comparable minimum eruption rate of 5.8×10^6 m^3/yr, but the rate for the deep-flow fields is not well determined because they may have been active after the lake covered their source. Likewise, the eruption rate of Merriam Cone is poorly known because of uncertainty in the duration of activity. Assuming that postcaldera

andesitic volcanism was over by the time the Wizard Island volcano ceased to erupt gives a minimum rate of 8.2×10^6 m^3/yr for the entire andesitic volume integrated over the maximum likely period given by the lake-filling model (Table 2).

Conversion of volume eruption rates to mass eruption rates allows comparison with historic lava effusion rates at arc volcanoes. Assuming an average bulk density of 2200 kg/m^3 for postcaldera andesite lava and breccia results in a minimum average long-term eruption rate for total postcaldera andesite of 580 kg/s. This rate is similar to long-term mean lava-effusion rates at arc volcanoes tabulated by Pyle (2000; e.g., Mount St. Helens (1980–1986)—700 kg/s; Santiaguito (1925–1984)—800 kg/s). If erupted in several events of short duration, which seems likely, postcaldera rates at Crater Lake still would be well within the range reported by Pyle (2000) for events lasting 1–5 yr (4000–150 000 kg/s).

CONCLUSIONS

The new high-resolution multibeam bathymetry reveals landforms beneath Crater Lake in striking detail. Ambiguities in interpretation of earlier bathymetry have been resolved and new features discovered. The high resolution of the new bathymetry leads to improved understanding of volcanic and sedimentary processes within the caldera lake and, what is even more important, to a chronology for the postcaldera geologic history. Major conclusions are as follows.

1. Postcaldera andesitic volcanism was synchronous with rapid filling of the lake and lasted at most a few hundred years. The vented 4 km^3 of andesite now makes up a subaqueous breccia cone, subaqueous lava flows, and several superimposed lava deltas capped by a subaerial cinder cone. Passage zones in the lava deltas record former lake levels and demonstrate concurrent eruptions at the Wizard Island and central-platform vents.

2. Extensive debris-avalanche deposits and well-developed debris aprons are present beneath embayments in the caldera wall. At least three of the debris avalanches postdate the andesitic postcaldera volcanoes and therefore were subaqueous. Secondary slides remobilized some of the debris-avalanche deposits.

3. Caldera-wall embayments are separated by promontories continuous with submerged bedrock outcrops, some correlative with exposed geologic units of Mount Mazama. The deepest outcrops circumscribe the ring-fracture system that forms the structural boundary of the foundered cauldron block.

4. Several drowned beaches are present wherever relatively fine, unconsolidated materials occur at shallow depth. The deepest beach approximately corresponds to the elevation of a lava surface below a permeable layer in the northeast caldera wall. The lake apparently filled rapidly to this elevation and then more gradually to the present level, the beaches reflecting climatic influences on lake level. A gently sloping wave-cut platform at 1877–1883 m elevation, commonly 40 m wide in easily eroded materials many places around the shore, indicates that Crater Lake has remained near its present level for a long time.

ACKNOWLEDGMENTS

We thank the staff of Crater Lake National Park and the U.S. Army Reserve, Fort Lewis, Washington, for enabling us to conduct the bathymetric survey of Crater Lake. The professionalism and expertise of the C and C Technologies, Inc. crew led to the high quality of the data. L. Hellequin was instrumental in the field data processing. M. Nathenson contributed substantially to documenting the drowned beaches and generously provided the model for filling of Crater Lake. We appreciate reviews by J. G. Moore and M. E. Reid of an early draft of the manuscript and journal reviews by R. W. Collier and L. G. Mastin. The survey of Crater Lake was made possible with financial support from Crater Lake National Park and from the U.S. Geological Survey Coastal and Marine Geology and Volcano Hazards Programs.

REFERENCES CITED

Bacon, C.R., 1983, Eruptive history of Mount Mazama and Crater Lake caldera, Cascade Range, U.S.A.: Journal of Volcanology and Geothermal Research, v. 18, p. 57–115.

Bacon, C.R., and Druitt, T.H., 1988, Compositional evolution of the zoned calcalkaline magma chamber of Mount Mazama, Crater Lake, Oregon: Contributions to Mineralogy and Peterology, v. 98, p. 224–256.

Bacon, C.R., and Lanphere, M.A., 1990, The geologic setting of Crater Lake, Oregon, *in* Drake, E.T., Collier, R., Dymond, J., and Larson, G.L., eds., Crater Lake: An ecosystems study: San Francisco, Pacific Division, American Association for the Advancement of Science, p. 19–27.

Bacon, C.R., and Nathenson, Manuel, 1996, Geothermal resources in the Crater Lake area, Oregon: U.S. Geological Survey Open-File Report OFR-96–663, 34 p.

Bacon, C.R., Mastin, L.G., Scott, K.M., and Nathenson, Manuel, 1997, Volcano and earthquake hazards in the Crater Lake region, Oregon: U.S. Geological Survey Open-File Report OFR-97–487, 32 pages.

Byers, F.M., Jr., 1959, Geology of Umnak and Bogoslof Islands, Aleutian Islands, Alaska: U.S. Geological Survey Bulletin 1028-L, p. 267–369.

Byrne, J.V., 1962, Bathymetry of Crater Lake, Oregon: Ore Bin, v. 24, p. 161–164.

Byrne, J.V., 1965, Morphometry of Crater Lake, Oregon: Limnology and Oceanography, v. 10, p. 462–465.

Carlisle, H., 1963, Pillow breccias and their aquagene tuffs, Quadra Island, B.C.: Journal of Geology, v. 71, p. 48–71.

Collier, R.W., Dymond, J., and McManus, J., 1991, Studies of hydrothermal processes in Crater Lake, OR: Corvallis, Oregon, Oregon State University College of Oceanography Report 90-7, 317 pages.

Crandell, D.R., Miller, C.D., Glicken, H.X., Christiansen, R.L., and Newhall, C.G., 1984, Catastrophic debris avalanche from ancestral Mount Shasta volcano: Geology, v. 12, p. 143–146.

Diller, J.S., and Patton, H.B., 1902, The geology and petrography of Crater Lake National Park: U.S. Geological Survey Professional Paper 3, 167 pages.

Druitt, T.H., and Bacon, C.R., 1986, Lithic breccia and ignimbrite erupted during the collapse of Crater Lake caldera, Oregon: Journal of Volcanology and Geothermal Research, v. 29, p. 1–32.

Dymond, J., and Collier, R.W., 1989, Bacterial mats from Crater Lake, Oregon and their relationship to possible deep-lake hydrothermal venting: Nature, v. 342, p. 673–675.

Fuller, R.E., 1931, The aqueous chilling of basaltic lava on the Columbia River Plateau: American Journal of Science, ser. 5, v. 21, p. 281–300.

Fytikas, M., Kolios, N., and Vougioukalakis, G., 1990, Post-Minoan volcanic activity of the Santorini volcano. Volcanic hazard and risk, forecasting possibilities, *in* Hardy, D.A., Keller, J., Galanopoulos, V.P., Flemming, N.C., and Druitt, T.H., eds., Thera and the Aegean world III: London, Thera Foundation, v. 2, p. 183–198.

Gardner, J.V., Field, M.E., Lee, H., Edwards, B.E.,, Masson, D.G., Kenyon, N., and Kidd, R.B., 1991, Ground truthing 6.5-kHz sidescan sonographs: What are we really imaging?: Journal of Geophysical Research, v. 96, p. 5955–5974.

Gardner, J.V., Mayer, L.A., and Hughes Clarke, J.E., 2000a, Morphology and processes in Lake Tahoe (California-Nevada): Geological Society of America Bulletin, v. 112, p. 736–746.

Gardner, J.V., Mayer, L.A., and Buktenica, M., 2000b, Cruise report RV *Surf Surveyor* Cruise S1–00-CL, Mapping the bathymetry of Crater Lake, Oregon: U.S. Geological Survey Open-File Report OFR-00-405, 32 p.

Gardner, J.V., Dartnell, P., Hellequin, L., Bacon, C.R., Mayer, L.A., Buktenica, M.W., and Stone, J.C., 2001, Bathymetry and selected perspective views of Crater Lake, Oregon: U.S. Geological Survey Water Resources Investigations Report WRI-01-4046, scale 1:15 000, 2 sheets.

Glicken, H., 1998, Rockslide-debris avalanche of May 18, 1980, Mt. St. Helens volcano, Washington: Bulletin of the Geological Survey of Japan, v. 49, p. 55–106.

Hildreth, W., 1996, Kulshan caldera: A Quaternary subglacial caldera in the North Cascades, Washington: Geological Society of America Bulletin, v. 108, p. 786–793.

Hughes Clarke, J.E., 1993, The potential for seabed classification using backscatter from shallow water multibeam sonars, *in* Pace, N., and Langhome, D.N., eds., Acoustic classification and mapping of the seafloor: Proceedings of the Institute of Acoustics, v. 15, p. 381–388.

Jones, J.G., and Nelson, P.H.H., 1970, The flow of basalt lava from air into water—Its structural expression and stratigraphic significance: Geological Magazine, v. 107, p. 13–19.

Krastel, S., Schmincke, H.-U., Jacobs, C.L., Rihm, R., Le Bas, T.P., and Alibés, B., 2001, Submarine landslides around the Canary Islands: Journal of Geophysical Research, v. 106, p. 3977–3997.

Lipman, P.W., 1997, Subsidence of ash-flow calderas: Relation to caldera size and magma-chamber geometry: Bulletin of Volcanology, v. 59, p. 198–218.

Macdonald, G.A., 1954, Activity of Hawaiian volcanoes during the years 1940–1950: Bulletin Volcanologique, v. 15, p. 119–179.

Mathews, W.H., 1947, ''Tuyas,'' flat-topped volcanoes in northern British Columbia: American Journal of Science, v. 245, p. 560–570.

Moore, J.G., Clague, D.A., Holcomb, R.T., Lipman, P.W., Normark, W.R., and Torresan,

M.E., 1989, Prodigious submarine landslides on the Hawaiian Ridge: Journal of Geophysical Research, v. 94, p. 17 465–17 484.
Nathenson, Manuel, 1992, Water balance for Crater Lake, Oregon: U.S. Geological Survey Open-File Report OFR-92–505, 33 pages.
Nathenson, Manuel, Bacon, C.R., and Gardner, J.V., 2001, Models for the filling of Crater Lake, Oregon [abs.]: Eos (Transactions, American Geophysical Union), v. 82, no. 47, Fall Meeting Supplement, p. F1376–F1377.
Nelson, C.H., 1967, Sediments of Crater Lake, Oregon: Geological Society of America Bulletin, v. 78, p. 833–848.
Nelson, C.H., Meyer, A.W., Thor, D., and Larsen, M., 1986, Crater Lake, Oregon: A restricted basin with base-of-slope aprons of nonchannelized turbidites: Geology, v. 14, p. 238–241.
Nelson, C.H., Carlson, P.R., and Bacon, C.R., 1988, The Mount Mazama climactic eruption (6900 BP) and resulting convulsive sedimentation on the continent, ocean basin, and Crater Lake caldera floor, *in* Clifton, H.E., ed., Sedimentologic consequences of convulsive geologic events: Geological Society of America Special Paper 229, p. 37–57.
Nelson, C.H., Bacon, C.R., Robinson, S.W., Adam, D.P., Bradbury, J.P., Barber, J.H., Jr., Schwartz, D., and Vagenas, G., 1994, The volcanic, sedimentologic and paleolimnologic history of the Crater Lake caldera floor, Oregon: Evidence for small caldera evolution: Geological Society of America Bulletin, v. 106, p. 684–704.
Peterson, D.L., Silsbee, D.G., and Redmond, K T., 1999, Detecting long-term hydrological patterns at Crater Lake, Oregon: Northwest Science, v. 73, p. 121–130.
Phillips, K.N., 1968, Hydrology of Crater, East, and Davis Lakes, Oregon, *with a section on* Chemistry of the lakes by Van Denburgh, A.S.: U.S. Geological Survey Water-Supply Paper 1859-E, 60 p.
Prior, D.B., Bornhold, B.D., Coleman, J.M., and Bryant, W.R., 1982, Morphology of a submarine slide, Kitimat Arm, British Columbia: Geology, v. 10, p. 588–592.
Pyle, D.M., 2000, Sizes of volcanic eruptions, *in* Sigurdsson, H., Houghton, B.F., McNutt, S.R., Rymer, H., and Stix, J., eds., Encyclopedia of volcanoes: New York, Academic Press, p. 263–269.
Redmond, K.T., 1990, Crater Lake climate and lake level variability, *in* Drake, E.T., Collier, R., Dymond, J., and Larson, G.L., eds., Crater Lake: An ecosystems study: San Francisco, Pacific Division, American Association for the Advancement of Science, p. 127–141.
Richards, A.F., 1959, Geology of the Islas Revillagigedo, Mexico. 1. Birth and development of Volcán Bárcena, Isla San Benedicto: Bulletin Volcanologique, v. 22, p. 73–123.
Siebert, L., 1984, Large volcanic debris avalanches: Characteristics of source areas, deposits, and associated eruptions: Journal of Volcanology and Geothermal Research, v. 22, p. 163–197.
Staudigel, H., and Schmincke, H.-U., 1984, The Pliocene seamount series of La Palma/Canary Islands: Journal of Geophysical Research, v. 89, p. 11 195–11 215.
Stine, S., 1990, Late Holocene fluctuations of Mono Lake, California: Palaeogeography, Palaeoclimatology, Palaeoecology, v. 78, p. 333–381.
Stuiver, M., and Reimer, P.J., 1993, Extended ^{14}C data base and revised CALIB 3.0 ^{14}C age calibration program: Radiocarbon, v. 35, p. 215–230.
Suzuki-Kamata, K., Kamata, H., and Bacon, C.R., 1993, Evolution of the caldera-forming eruption at Crater Lake, Oregon, indicated by component analysis of lithic fragments: Journal of Geophysical Research, v. 98, p. 14 059–14 074.
Thorarinsson, S., 1967, Surtsey, the new island in the North Atlantic: New York, Viking Press, 54 p. (translated by S. Eysteinsson).
Ui, T., 1983, Volcanic dry avalanche deposits—Identification and comparison with nonvolcanic debris stream deposits: Journal of Volcanology and Geothermal Research, v. 18, p. 135–150.
Wheat, C.G., McManus, J., Dymond, J., Collier, R., and Whiticar, M., 1998, Hydrothermal fluid circulation through the sediment of Crater Lake, Oregon: Pore water and heat flow constraints: Journal of Geophyscial Research, v. 103, p. 9931–9944.
Williams, H., 1942, The geology of Crater Lake National Park, Oregon: Carnegie Institution of Washington Publication 540, 162 pages.
Williams, H., 1961, The floor of Crater Lake, Oregon: American Journal of Science, v. 259, p. 81–83.
Williams, D.L., and Von Herzen, R.P., 1983, On the terrestrial heat flow and physical limnology of Crater Lake, Oregon: Journal of Geophysical Research, v. 88, p. 1094–1104.
Yamagishi, H., 1991, Morphological and sedimentological characteristics of the Neogene submarine coherent lavas and hyaloclastites in southwest Hokkaido, Japan: Sedimentary Geology, v. 74, p. 5–23.

MANUSCRIPT RECEIVED BY THE SOCIETY JULY 20, 2001
MANUSCRIPT ACCEPTED JANUARY 8, 2002

Printed in the USA